Cell Metabolism

Article

Cellular deconstruction of the human skeletal muscle microenvironment identifies an exercise-induced histaminergic crosstalk

Graphical abstract

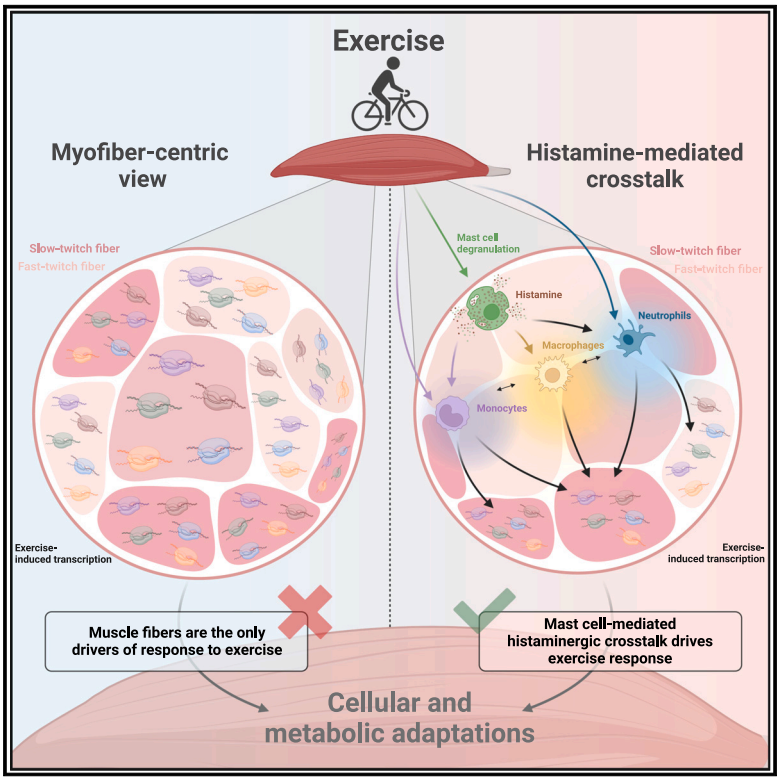

Highlights

- Mononuclear cells are primary drivers of the exercise response in skeletal muscle
- Release of histamine from skeletal muscle during exercise from mast cells
- Histamine receptor antagonists impair post-exercise muscle glycogen resynthesis
- Exercise-induced transcriptional activation of inflammatory signaling by histamine

Authors

Thibaux Van der Stede, Alexia Van de Loock, Guillermo Turiel, ..., Jo Vandesompele, Katrien De Bock, Wim Derave

Correspondence

wim.derave@ugent.be

In brief

Van der Stede et al. identified a role for mononuclear cells in the skeletal muscle microenvironment to steer the response to exercise. Mast cells locally secrete histamine during exercise, triggering activation of H1 and H2 receptors on myeloid and vascular cells, thereby affecting the exercise-induced metabolic and transcriptional adaptive response.

Van der Stede et al., 2025, Cell Metabolism *37*, 842–856
April 1, 2025
https://doi.org/10.1016/j.cmet.2024.12.011

CellPress

CellPress
OPEN ACCESS

Cell Metabolism

Article

Cellular deconstruction of the human skeletal muscle microenvironment identifies an exercise-induced histaminergic crosstalk

Thibaux Van der Stede,[1,2,9] Alexia Van de Loock,[1,9] Guillermo Turiel,[3] Camilla Hansen,[2] Andrea Tamariz-Ellemann,[2] Max Ullrich,[1] Eline Lievens,[1] Jan Spaas,[1,4] Nurten Yigit,[5] Jasper Anckaert,[5] Justine Nuytens,[5] Siegrid De Baere,[6] Ruud Van Thienen,[1] Anneleen Weyns,[1] Laurie De Wilde,[7] Peter Van Eenoo,[7] Siska Croubels,[6] John R. Halliwill,[8] Pieter Mestdagh,[5] Erik A. Richter,[2] Lasse Gliemann,[2] Ylva Hellsten,[2] Jo Vandesompele,[5] Katrien De Bock,[3] and Wim Derave[1,10,*]

[1]Department of Movement and Sports Sciences, Ghent University, Ghent, Belgium
[2]Department of Nutrition, Exercise and Sports, University of Copenhagen, Copenhagen, Denmark
[3]Laboratory of Exercise and Health, Department of Health Sciences and Technology, Swiss Federal Institute of Technology (ETH Zürich), Zurich, Switzerland
[4]BIOMED Biomedical Research Institute, Faculty of Medicine and Life Sciences, Hasselt University, Diepenbeek, Belgium
[5]OncoRNALab, Department of Biomolecular Medicine, Ghent University, Ghent, Belgium
[6]Laboratory of Pharmacology and Toxicology, Department of Pathobiology, Pharmacology and Zoological Medicine, Ghent University, Merelbeke, Belgium
[7]Department of Diagnostic Sciences, Doping Control Laboratory, Ghent University, Ghent, Belgium
[8]Bowerman Sports Science Center, Department of Human Physiology, University of Oregon, Eugene, OR, USA
[9]These authors contributed equally
[10]Lead contact
*Correspondence: wim.derave@ugent.be
https://doi.org/10.1016/j.cmet.2024.12.011

SUMMARY

Plasticity of skeletal muscle is induced by transcriptional and translational events in response to exercise, leading to multiple health and performance benefits. The skeletal muscle microenvironment harbors myofibers and mononuclear cells, but the rich cell diversity has been largely ignored in relation to exercise adaptations. Using our workflow of transcriptome profiling of individual myofibers, we observed that their exercise-induced transcriptional response was surprisingly modest compared with the bulk muscle tissue response. Through the integration of single-cell data, we identified a small mast cell population likely responsible for histamine secretion during exercise and for targeting myeloid and vascular cells rather than myofibers. We demonstrated through histamine H1 or H2 receptor blockade in humans that this paracrine histamine signaling cascade drives muscle glycogen resynthesis and coordinates the transcriptional exercise response. Altogether, our cellular deconstruction of the human skeletal muscle microenvironment uncovers a histamine-driven intercellular communication network steering muscle recovery and adaptation to exercise.

INTRODUCTION

Skeletal muscle comprises 40% of the human body weight, consisting of multinucleated muscle fibers and multiple other mononuclear cell types. The swift remodeling of skeletal muscle in response to exercise induces training adaptations (e.g., mitochondrial biogenesis) that drive many health-promoting benefits (e.g., increased insulin sensitivity).[1] High-intensity interval training (HIIT) is generally superior in improving the aerobic capacity of an individual compared with moderate-intensity continuous training, although it is unclear how exercise intensity dictates the cellular adaptations in skeletal muscle.[2] Earlier studies have focused on how exercise intensity affects muscle gene expression,[3,4] phosphoregulation of the muscle proteome,[5] and biosynthesis of signaling metabolites.[6]

Despite these important endeavors, the rich cell diversity in skeletal muscle and its relation to the adaptive response to exercise have not yet received their warranted attention. Muscle fibers are the dominant cells in skeletal muscle, generally classified as "slow" and "fast" fibers,[7] with substantial differences in the exercise response between both fiber types.[8,9] Next to the myofibers, an important role for regulation of muscle homeostasis and plasticity can be ascribed to the various residing or infiltrating mononuclear cells. Bulk transcriptomics datasets have made it clear that there is a vast transcriptional landscape of exercise responses and that knowledge on most of the canonical

CellPress
OPEN ACCESS

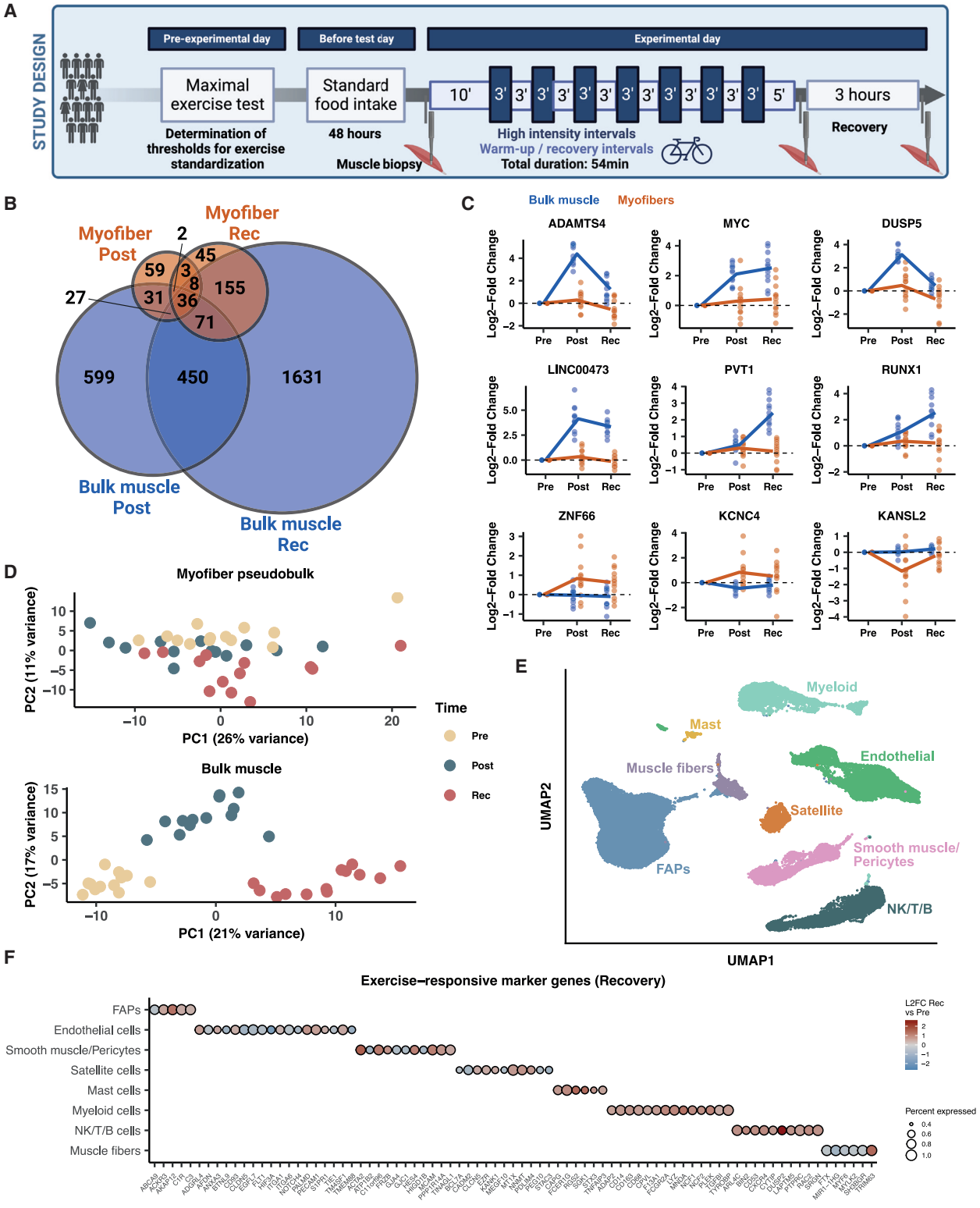

Figure 1. Contribution of non-muscle cells to the adaptive response to exercise

(A) Overview of experimental design for the acute human exercise intervention.

(B) Overlap between myofiber-specific and bulk muscle DEGs after HIIT.

(C) Expression time profile of selected genes for myofibers and bulk muscle, including individual data points (n = 12).

(legend continued on next page)

exercise-induced genes is insufficient.[10] These bulk muscle resources are limited, however, in their ability to disentangle the contributions of specific cell types. The introduction of various single-cell omics technologies in skeletal muscle research has been transforming our view on the heterogeneity and importance of mononuclear non-muscle cells,[11–13] but they have up until now mainly been used to study skeletal muscle regeneration. For example, endothelial cells[14] and fibroblasts[15] control muscle regeneration after limb ischemia via crosstalk with macrophages. While some groups have started to explore this emerging field,[16] more work is required to understand exercise adaptations from a multicellular perspective.

Mast cells, a myeloid cell type that has been largely overlooked in relation to skeletal muscle, might be one cell type involved in exercise-induced intercellular crosstalk. Mast cells may communicate to neighboring cells upon degranulation with exercise and subsequent release of histamine,[17,18] but necessary evidence is lacking. Here, we show, in humans, that the exercise-induced transcriptional response of myofibers constitutes only a fraction of the total exercise transcriptome in bulk muscle, conveying a large unaccounted role for mononuclear cells. In these, we identified a small mast cell population alongside a potent paracrine histamine release in human muscle during exercise. Experiments with selective blockade of histamine receptors indicate a histaminergic control of metabolic recovery and remodeling of human muscle.

RESULTS

Contribution of non-muscle cells to the adaptive response to exercise

To start exploring the role of mononuclear non-muscle cells in exercise responses, we applied two transcriptome profiling strategies to skeletal muscle biopsies collected before and after high-intensity interval exercise in young, healthy individuals (12M/2F, 22–42 years old). We first performed bulk muscle total RNA sequencing (RNA-seq), as this readout comprises both the myofibers and the different mononuclear non-muscle cells (e.g., endothelial cells, fibro-adipogenic progenitors [FAPs], and macrophages). Secondly, we employed our recently described single-fiber poly(A+) transcriptome profiling method,[19] yielding insights in the myofiber-specific response. The biopsies were collected before high-intensity interval cycling exercise (exercise duration: 54 min), immediately after, and after 3 h of recovery (Figure 1A). After stringent quality control, the myofiber dataset comprised 912 high-quality fibers (70 fibers on average per participant, Figure S1A). Between the myofiber and bulk muscle dataset, there was a 93% overlap in the number of detected genes (Figure S1B), a similar distribution of transcript biotypes (coding, long non-coding, or antisense) (Figure S1C), as well as a high correlation (r = 0.729) in expression of common genes (Figure S1D). There was a reasonable overlap between exercise-induced differentially expressed genes (DEGs) at a myofiber-specific level versus bulk muscle, although the number of DEGs was much higher in bulk muscle (Figure 1B; Table S1). Induction of several "core" exercise-responsive genes (*PPARGC1A*, *NR4A3*, *EGR1*, *FOS*, *JUNB*, and *ANKRD1*) was similar in myofibers versus bulk muscle and similar to the MetaMEx database[10] (Figure S1E). However, many features showed a divergent response, such as the metalloproteinase *ADAMTS4*,[20] the transcription factor *MYC*,[21] and the non-coding *LINC00473*, which were strongly upregulated only in bulk muscle (Figure 1C). Genes such as *ZNF66*, *KCNC4*, and *KANSL2*, on the other hand, only showed exercise-induced up- or downregulation in myofibers. To further compare myofibers versus bulk muscle, we performed principal-component analysis (PCA) on the complete dataset of resting, post-exercise, and recovery biopsies. Samples showed a moderate separation by time point, and only along PC2, in the myofiber-specific samples, while the exercise-induced separation in the PCA plot was very pronounced along PC1 in bulk muscle (Figure 1D).

These comparisons of exercise-induced effects in myofibers versus bulk muscle showed that the transcriptional response of bulk muscle is much more pronounced. Although these differences could be partly related to a lower sequencing depth of the myofiber-specific samples, another mechanism could be that the different mononuclear non-muscle cells, either resident or infiltrating, harbor a profound potential to affect the skeletal muscle response to exercise. To start appreciating the role of this cell diversity, we integrated our single-fiber dataset of 925 fibers at rest[19] with a single-cell dataset (4 participants, 37,333 cells) of human skeletal muscle.[22] This approach is unique in its ability to study the complete human skeletal muscle niche, as compared with widely available single-cell (only mononuclear cells) or single-nuclei (only nuclear RNA and >85% myonuclear RNA) transcriptome methods. By annotating the different clusters obtained after integration with well-known marker genes for different cell types (Figure S1F), we could identify eight general categories of different cell types, including FAPs, vascular cells (smooth muscle/pericytes and endothelial), muscle fibers, satellite cells, and immune cells (mast cells, other myeloid cells, and natural killer [NK]/T/B cells) (Figure 1E). As a first step in exploring the contribution of these mononuclear cell populations to the adaptive response to exercise, we interrogated if the specific marker genes of the different cell populations are up- or downregulated in the bulk muscle exercise dataset. While this analysis does not discern if there is an infiltration of immune cells or an upregulation of genes within resident cells, it could represent the plastic nature of marker genes for non-muscle cells. Indeed, many of the marker genes are present in the bulk muscle DEG lists, especially immune and vascular cell markers at both post-exercise (Figure S1G) and recovery (Figure 1F). Marker

(D) Principal-component analysis for myofibers and bulk muscle. Each dot represents one participant and is colored by time point (pre-exercise, post-exercise, or recovery) (n = 13).
(E) Integrated UMAP of mononuclear cells and muscle fibers of human skeletal muscle.
(F) Dot plot of the intersection of genes for the DEGs from the bulk muscle exercise dataset (at recovery versus pre-exercise) with the cell identifier genes for the different populations from the single-cell dataset (top 50 genes per cell type). Color and size of the dots depict exercise-induced change in gene expression (bulk muscle dataset) and percentage of cells expressing the gene (single-cell dataset), respectively.
See also Table S1.

CellPress
OPEN ACCESS

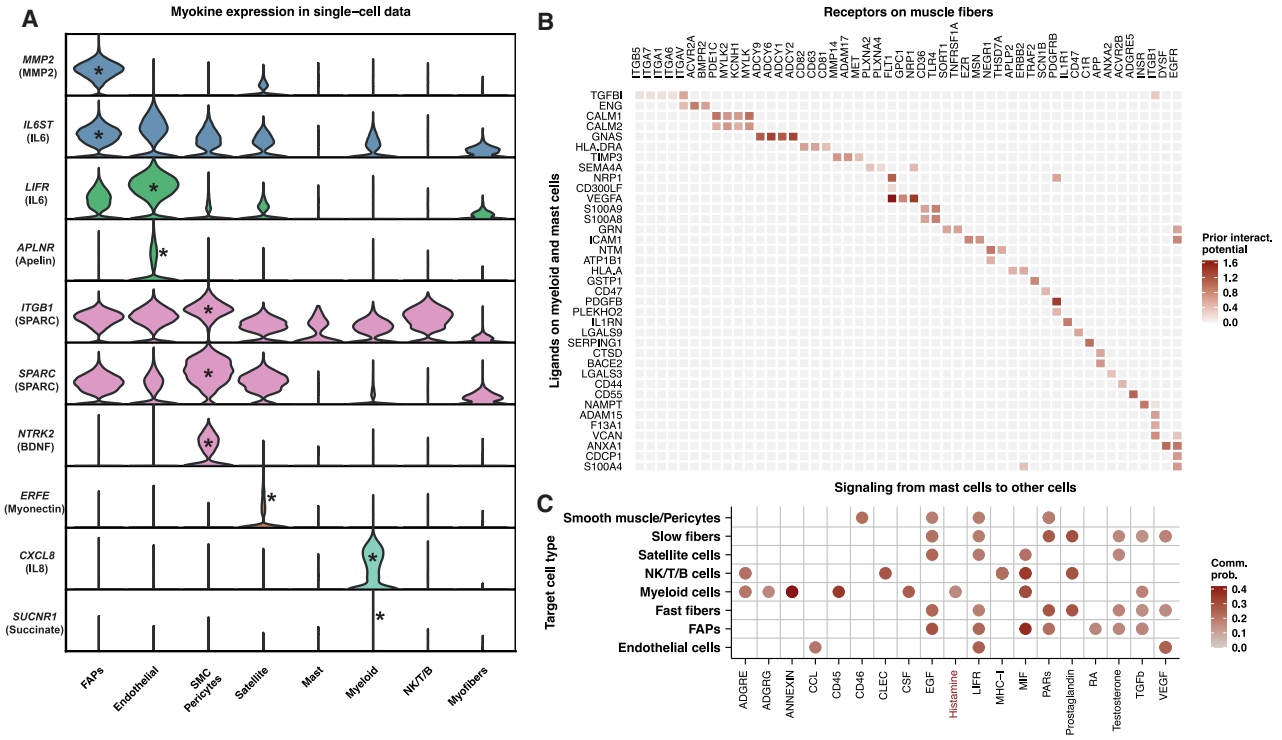

Figure 2. Extensive intercellular communication networks in the skeletal muscle niche

(A) Violin plots depicting expression of known myokines and their receptors in the integrated single-cell/fiber dataset. Asterisks and colors indicate significant enrichment of this gene in the respective cell type.

(B) NicheNet results illustrating the interaction potential of ligands expressed in myeloid cells and their downstream receptors expressed in muscle fibers.

(C) CellChat results of communication pathways from mast cells to other cell types.

genes for the muscle fibers were largely unaffected by exercise. These data suggest a potential role for mononuclear non-muscle cells in regulating exercise responses in skeletal muscle.

Extensive intercellular communication networks in the skeletal muscle niche

After integrating our comprehensive dataset containing all cell types in human skeletal muscle, we wondered if we could profile novel cell-cell communication networks in the skeletal muscle microenvironment.[23] We started with a targeted approach focusing on known secreted myokines involved in intercellular and interorgan crosstalk and potentially important for driving exercise adaptations.[24,25] Capitalizing on this prior knowledge, we mapped several myokines or their receptors across the different cell types in our single-cell/fiber dataset to further understand their role in the muscle microenvironment (Figure 2A). Matrix metalloproteinase-2 (*MMP2*), likely important for extracellular matrix remodeling,[26] was exclusively expressed in FAPs, while FAPs and endothelial cells showed the highest expression for the interleukin (IL)-6/LIF (leukemia inhibitory factor) receptors gp130 (*IL6ST*) and *LIFR*.[27] Vascular cells were also the main contributors for the apelin receptor (*APLNR*),[28] secreted protein acidic and rich in cysteine (*SPARC*), and its presumable target receptor integrin β1 (*ITGB1*),[29] and the receptor for brain-derived neurotrophic factor (BDNF) (*NTRK2*).[30] Myonectin (*CTRP15/ERFE*), potentially involved in the control of cellular autophagy, was mainly expressed in satellite cells.[31] Myeloid cells were enriched for several features such as IL-8 (*CXCL8*)[32] and the receptor for succinate signaling, *SUCNR1*.[33,34] Altogether, this analysis further underscores the importance of various non-muscle cells for their contribution to myokine-mediated responses.[35]

Leveraging the strength of the integrated single-fiber and single-cell dataset, we then employed a more global approach with NicheNet.[36] This cell-cell communication tool allows us to get a better understanding of intercellular communication networks that may be active during exercise. For this analysis, we used the bulk muscle DEGs at both post-exercise and recovery to predict related ligand-receptor pairs and the (in)activation of their downstream targets, independent of fiber type. We specifically focused on the communication from the myeloid cluster (macrophages, monocytes, dendritic cells [DCs], and neutrophils) and mast cells to muscle fibers, since recent evidence is starting to unravel the essential role of inflammatory signaling for exercise-induced adaptations of skeletal muscle.[37] NicheNet identified a multitude of active ligands expressed on these myeloid cells, connected in an intertwined signaling network with their receptors expressed on muscle fibers (Figure 2B). These involved transforming growth factor β signaling (*TGF-B*), which is involved in skeletal muscle regeneration,[38] functioning via macrophages and several integrins expressed on muscle fibers. Several other communication networks, such as *ANXA1-DYSF* via mast cells or neutrophil-induced inflammatory signaling via

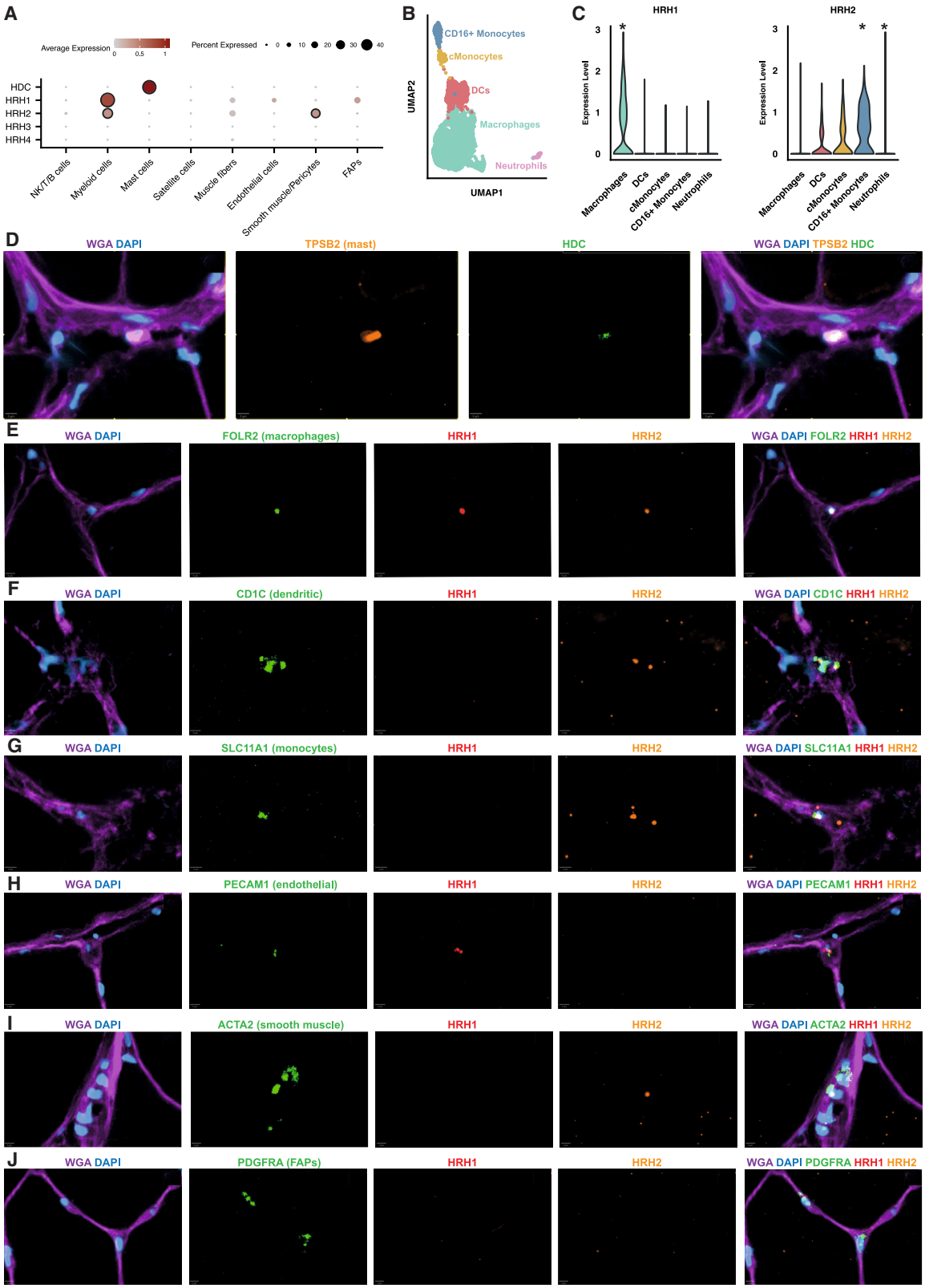

Figure 3. Histamine receptors are expressed on mononuclear non-muscle cells in human skeletal muscle

(A) Expression of histamine receptors and HDC in the integrated single-cell/fiber dataset. A black border indicates significant enrichment of this gene in the respective cell type.

(legend continued on next page)

S100A9/S100A8-TLR4, could all be involved in the intercellular communication in the muscle microenvironment. This approach to infer cell-cell communication networks can predict novel ligand-receptor pairs and signaling pathways that are potentially relevant for the adaptive response to exercise and could serve as a resource for future research.

Of particular interest was the presence of a small mast cell population in our dataset, which has been reported in some[39,40] but not other[12,41] previously published single-cell datasets on human skeletal muscle. Mast cells are granulocytes and tissue-residing upon differentiation, but little is known about their specific role in skeletal muscle, especially in relation to exercise responses. To start exploring this, we performed a CellChat analysis,[42] which can be used complementary to NicheNet, with the focus on signaling networks from mast cells to other cell types in the skeletal muscle niche. Multiple pathways were identified with this approach, for example, epidermal growth factor (EGF) signaling from mast cells to muscle fibers, previously shown to be involved in muscle mass regulation[43] (Figure 2C). Another potentially interesting network originating in mast cells is via histamine, signaling to myeloid cells as identified by CellChat (indicated in red). Histamine is mainly known for its role in allergies, although we and others have previously shown that the histamine signaling system also plays an essential role in driving the adaptive chronic response (aerobic capacity, insulin sensitivity, and microvascular function) to exercise training in humans.[17,18] We thus decided to further unravel how this histamine signaling pathway is functioning in skeletal muscle.

Histamine receptors are expressed on mononuclear non-muscle cells in human skeletal muscle

Upon their activation, mast cells degranulate and release inflammatory cytokines, histamine, and proteases.[44] Histamine is an evolutionary old signaling molecule, produced by decarboxylation of the semi-essential amino acid L-histidine via histidine decarboxylase (*HDC*), and functioning via four known G protein-coupled receptors termed H1-H4.[45] To further understand how mast cells and histamine contribute to the exercise response, we first assessed the expression of *HDC* and the specific histamine receptors in our integrated single-cell/fiber dataset. HDC appeared to be specific for this small mast cell population, indicating that mast cells are probably the unique histamine producers in human skeletal muscle (Figure 3A). There was no significant expression of histamine receptors on the muscle fibers, suggesting that histamine signaling in skeletal muscle is dependent on paracrine signaling among mononuclear non-muscle cells (Figure 3A). Histamine H1 receptors were significantly enriched in myeloid cells, with a lower (and non-significant) expression in endothelial cells and FAPs (Figure 3A). Histamine H2 receptors were significantly expressed on myeloid cells and smooth muscle cells. Histamine H3 and H4 receptors, however, were not expressed in skeletal muscle, confirming the hypothesis that H1 and H2 receptors are the main drivers for histamine signaling in skeletal muscle.[17] To further unravel the specific expression patterns in the rather general myeloid cell population, we extracted only these cells from the complete dataset and applied the same clustering pipeline as before. We could identify macrophages, DCs, neutrophils, and two monocyte populations (i.e., classical monocytes [cMonocytes] and CD16+ monocytes) (Figures 3B and S2A). Closer inspection of histamine receptor expression in these clusters showed that H1 receptors are significantly enriched in macrophages, whereas H2 receptor expression is significantly higher in $CD16^{+}$ monocytes and neutrophils (Figure 3C).

To validate the single-cell/fiber data, we performed an extensive RNAscope screen on cryosections of healthy human skeletal muscle biopsies. We selected specific markers for the different cell types based on the single-cell data: *TPSB2* (mast cells), *FOLR2* (macrophages), *CD1C* (DCs), *SLC11A1* (monocytes), *PECAM1* (endothelial cells), *ACTA2* (smooth muscle cells), and *PDGFRA* (FAPs). We could confirm that *HDC* is exclusively expressed in mast cells (Figures 3D and S2B). Macrophages consistently exhibited expression of both H1 and H2 receptors (Figures 3E and S2C), although the single-cell data suggested that mainly H1 receptors are expressed on macrophages. For both DCs and monocytes, we observed cells with H2 expression (consistent with single-cell data) and a considerable fraction without any histamine receptor expression (Figures 3F, 3G, S2D, and S2E). The vascular cells were mainly enriched for H1 receptors (endothelial cells) or H2 receptors (smooth muscle cells), although some cross-over was observed for smooth muscle cells (Figures 3H, 3I, S2F, and S2G). FAPs did not show any expression of histamine receptors, suggesting that these are likely not involved in the histamine signaling cascade (Figures 3J and S2H). Importantly, these images show almost no expression of H1 and little expression of H2 receptor on muscle fibers, confirming that histamine mainly acts on myeloid and vascular cells in the skeletal muscle microenvironment.

Local exercise-induced histamine release in the human skeletal muscle microenvironment

The histamine-producing activity of mast cells is likely activated by exercise, as the enzymatic activity of HDC is increased in rodents during exercise-like activities.[46,47] This is in accordance with data on known regulators of HDC activity, such as pH,[48] temperature,[49] and hypoxia,[50] all of which are also affected during exercise. Since we observed that *HDC* is exclusively expressed in mast cells in skeletal muscle and that the targeted histamine receptors are mainly expressed on myeloid and vascular cells, we next wondered if histamine could coordinate responses to exercise via mononuclear non-muscle cell crosstalk in the skeletal muscle microenvironment. We thus wanted to explore in detail if histamine levels are elevated in the skeletal muscle microenvironment during exercise, as has been suggested before.[51,52] We not

(B) Subclustering of myeloid cell cluster, visualized as UMAP.
(C) Violin plots indicating expression of histamine receptor H1 (HRH1) and H2 (HRH2) in the myeloid cells. Asterisks indicate significant enrichment of this gene in the respective cell type.
(D–J) RNAscope images of co-expression of *HDC* and histamine receptors (*HRH1* and *HRH2*) with mast cells (*TPSB2*), macrophages (*FOLR2*), DCs (*CD1C*), monocytes (*SLC11A1*), endothelial cells (*PECAM1*), smooth muscle cells (*ACTA2*), or FAPs (*PDGFRA*). Scale bars, 5 μm.

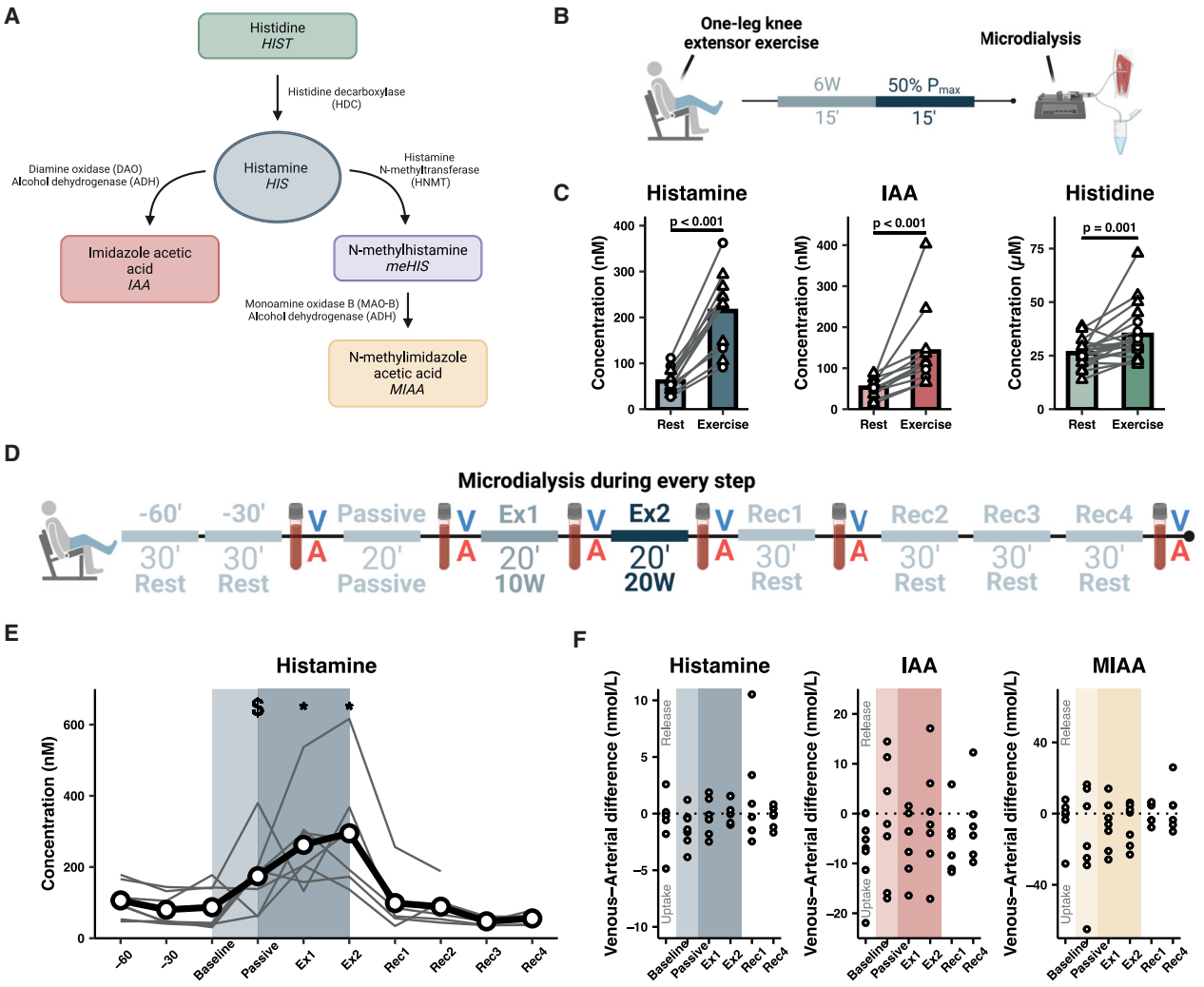

Figure 4. Local exercise-induced histamine release in the human skeletal muscle microenvironment

(A) Visual illustration of histamine metabolism pathway.

(B) Visual illustration of design for histamine release experiment.

(C) Interstitial levels of histamine, IAA, and histidine at rest and during exercise. Circles and triangles represent samples from young and older participants, respectively (n = 12).

(D) Visual illustration of design for histamine release experiment.

(E) Interstitial levels of histamine at each time point (n = 7).

(F) Difference in histamine, IAA, and MIAA levels between venous and arterial blood (n = 7).

only focused on histamine but also on its precursor histidine and its breakdown products imidazole acetic acid (IAA), N-methylhistamine (meHIS), and N-methylimidazole acetic acid (MIAA) (Figure 4A). Firstly, interstitial fluid from human muscle was collected in a separate experiment on younger and older individuals during one-leg knee-extensor exercise (Figure 4B). Histamine, IAA, and histidine all consistently increased during exercise, independent of age (Figure 4C). MIAA could not be reliably quantified, and MeHIS was undetected. To verify these results and to better understand the temporal nature, we performed a follow-up experiment on a separate cohort of healthy, young males, including sampling during passive exercise and during recovery (Figure 4D). Histamine and IAA were confirmed to increase in the muscle interstitium during active exercise and quickly returned to baseline upon cessation of exercise (Figures 4E and S3A). Histidine levels did not change in this experiment (Figure S3B). To evaluate a potential further release of interstitial histamine into the circulation, we also collected femoral arterial and venous blood samples in this human experiment. However, no release (A-V difference) of histamine or breakdown products (IAA and MIAA) could be observed (Figure 4F). This was confirmed in an independent experiment with a similar setup in post-menopausal women (Figure S3C). Altogether, these data show a clear and consistent local release of histamine into the muscle microenvironment upon exercise.

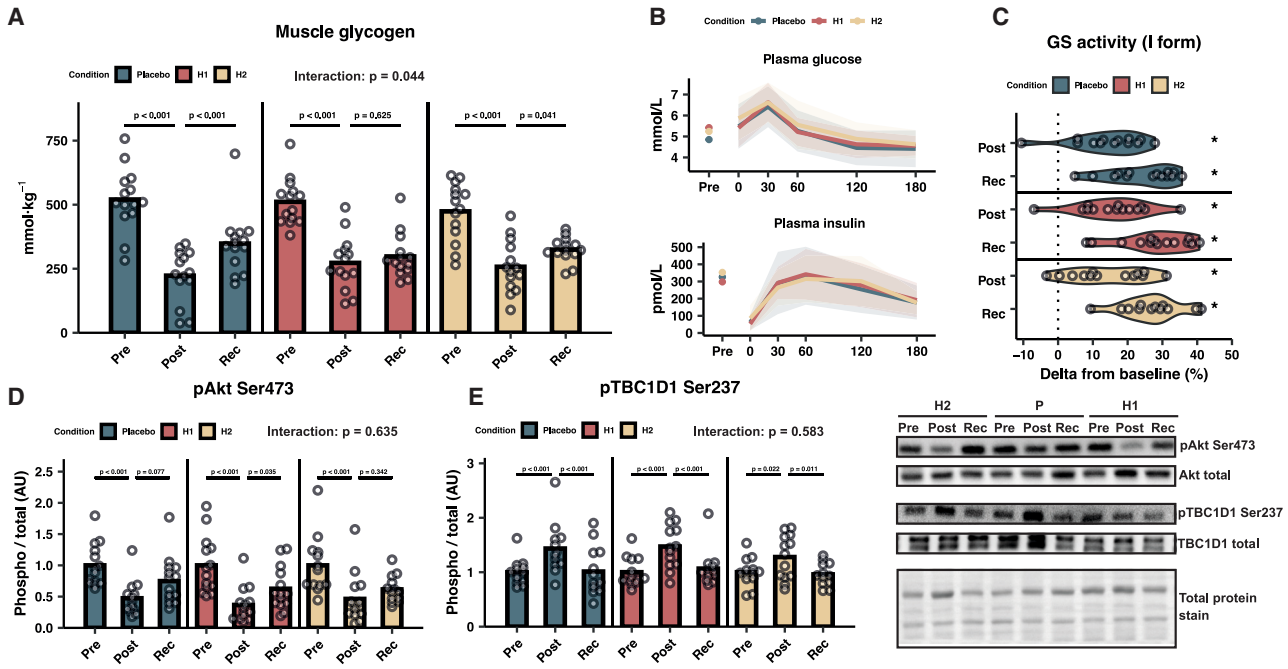

Figure 5. Histamine promotes post-exercise muscle glycogen resynthesis

(A) Muscle glycogen concentration pre-exercise (Pre), post-exercise (Post), and after 3 h of recovery (Rec) for placebo, H1 blockade, and H2 blockade (n = 14).

(B) Plasma glucose and insulin concentrations pre-exercise and at different time points during recovery (n = 14).

(C) Changes in glycogen synthase (GS) activity (I form) at post-exercise and recovery for each condition (n = 14).

(D and E) Phosphorylation levels of (D) AKT at Ser473 and (E) TBC1D1 at Ser237 at each time point (n = 14).

Histamine promotes post-exercise muscle glycogen resynthesis

We then sought to study the role of exercise-induced histamine and of its receptors in human muscle by oral administration of over-the-counter antihistamine medication. Clinically, histamine H1 and H2 receptor antagonists are used to treat allergy symptoms and gastric ulcers, respectively. Since our data showed that H1 and H2 receptors are expressed on distinct immune and vascular cell subtypes, we performed a human exercise study with either blockade of H1 or H2 receptors (or placebo). We collected muscle biopsies before high-intensity interval exercise, immediately after, and after 3 h of recovery (Figure S4A). An adequate metabolic control is essential during the recovery phase after exercise,[53] and an immune cell-mediated regulation of the skeletal muscle niche has been linked to glucose metabolism.[54] One of the hallmarks of muscle metabolic recovery after exhausting exercise is the capacity to replenish intracellular glycogen stores, which is dependent on optimal glucose delivery, uptake, and processing.[53] Hence, we queried if histamine is involved in glucose metabolism during and after exercise in humans. The results of this experiment showed that muscle glycogen utilization during exercise did not differ between the three conditions (placebo, H1 blockade, or H2 blockade). The resynthesis of glycogen during the 3-h recovery window, however, was impaired with H1 receptor blockade but not with H2 receptor blockade (Figure 5A). Overall circulating levels of glucose and insulin were not affected by histamine receptor blockade, confirming a similar glucose ingestion and availability (Figure 5B).

As glycogen resynthesis is a key component of adequate recovery from exercise, we first questioned if the activity of glycogen synthase, the main enzyme responsible for glycogen synthesis, was affected by histamine receptor blockade. The clear exercise-induced (post-exercise) and additive carbohydrate-induced (recovery) increases were similar between the conditions (Figures 5C and S4B). This was further confirmed by similar reductions in phosphorylation status, leading to the enzymatic activation of glycogen synthase (Figures S4C and S4D). We then probed for well-described targets of the canonical insulin signaling pathway that lead to GLUT4 translocation and increased glucose disposal in skeletal muscle.[55] Phosphorylation of targets related to proximal insulin signaling at the level of AKT was also not different between conditions (Figures 5D and S4E). Similar results were observed for the phosphoregulation of the Rab GTPases TBC1D4 and TBC1D1, downstream targets of AKT (Figures 5E, S4F, and S4G). Thus, histamine drives post-exercise muscle glycogen synthesis via H1 receptor signaling, independent of insulin-mediated activation of glycogen synthase and canonical insulin signaling.

Histamine mediates exercise-induced transcriptional activation of inflammatory signaling

Because canonical insulin signaling targets were not affected by histamine receptor blockade, we next focused on alternative exercise-induced signaling events. The metabolic stress sensor AMPK and its direct substrate acetyl-coenzyme A (CoA) carboxylase (ACC) were consistently phosphorylated by exercise, independent of histamine receptor blockade (Figures S5A and S5B).

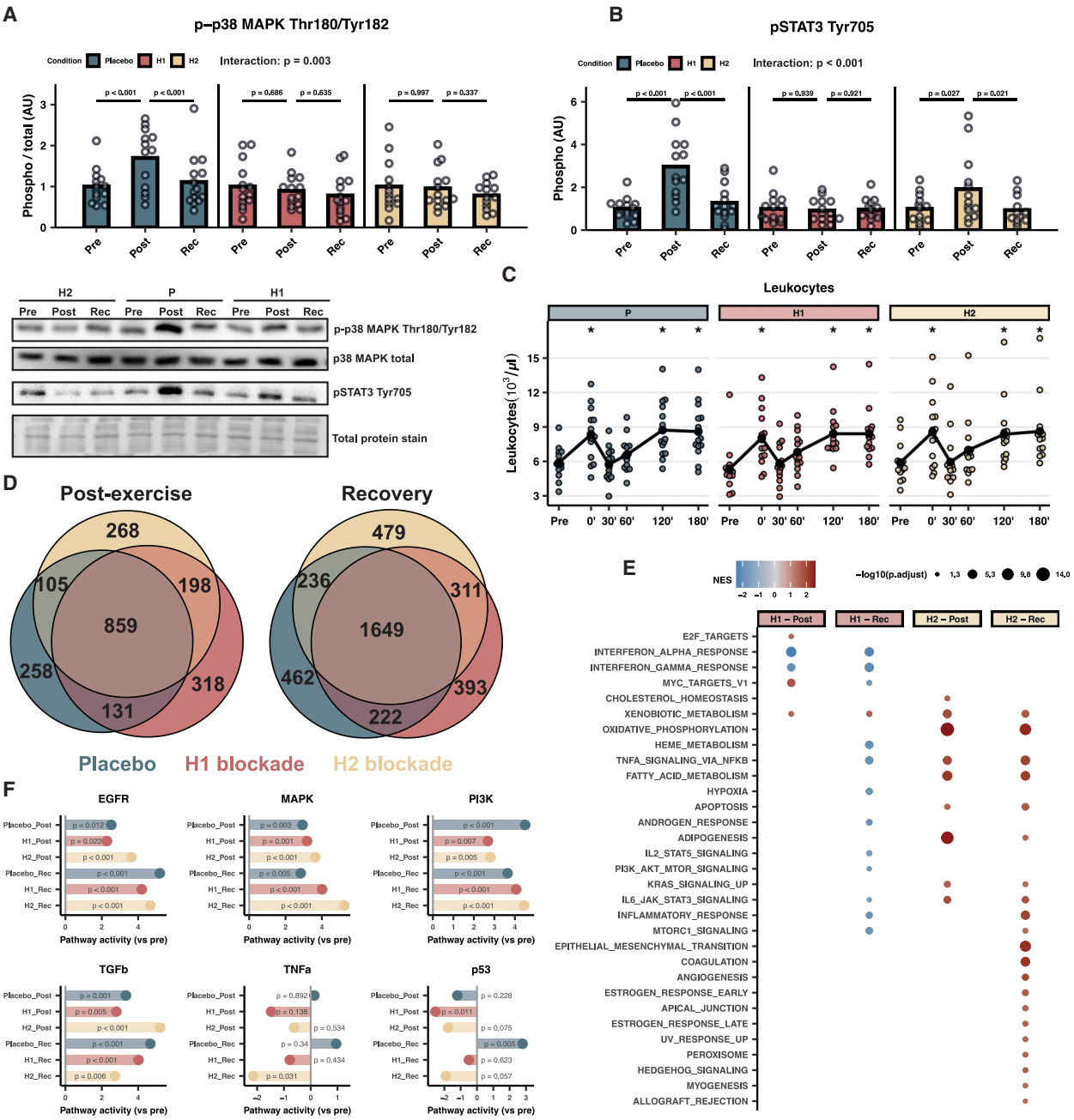

Figure 6. Histamine mediates exercise-induced transcriptional activation of inflammatory signaling

(A and B) Phosphorylation levels of (A) p38 MAPK at Thr180/Tyr182 and (B) STAT3 at Tyr705 at each time point (n = 14).

(C) Time profile of blood leukocytes before and after the HIIT exercise in the placebo, H1 blockade, and H2 blockade condition (n = 14).

(D) Overlap of bulk muscle DEGs at post-exercise and during recovery for each condition.

(E) GSEA comparing H1 or H2 blockade versus placebo at post-exercise and recovery using the Hallmark database on the bulk muscle dataset.

(F) Pathway activity inference on the single-fiber dataset for each condition at post-exercise and recovery.

See also Tables S2, S3, S4, S5, and S6.

Mitogen-activated protein kinases (MAPKs) are important regulators of metabolic control and muscle signaling in response to oxidative and energetic stress.[56,57] The exercise-induced activation of p38 MAPK was blunted with both H1 and H2 receptor blockade (Figure 6A), an effect not observed for ERK activation (Figure S5C). Activation of p38 MAPK in skeletal muscle is related to inflammatory processes and cytokine production.[57,58] We also observed a blunting with H1 blockade of the consistent exercise-induced phosphorylation of STAT3 (Figure 6B), related to inflammatory processes and activated by multiple cytokines

(e.g., IL-6) and growth factors (e.g., insulin growth factor [IGF]-1).[59] This is consistent with blunted induction of IL-6 with combined H1/H2 blockade.[60] We could, however, not detect an activation of the inflammatory p65 subunit of nuclear factor κB (NF-κB) (Figure S5D). Altogether, these results suggest that histamine might be involved in the exercise-induced inflammatory signaling in skeletal muscle.

We first confirmed that the paracrine histamine-mediated signaling events are restricted to the skeletal muscle niche, as suggested by the absence of a systemic histamine secretion (Figure 4). Indeed, histamine receptor antagonism did not affect the exercise-induced temporal changes in circulating immune cells (Figures 6C and S6A–S6E). We thus turned to our skeletal muscle samples before and after exercise and employed a global approach to assess transcriptional regulation of exercise-induced events by using bulk muscle RNA-seq. A similar number of total DEGs at both post-exercise (±1,500 genes) and recovery (±2,500 genes) were observed between the three conditions (Table S2). However, a considerable fraction of these DEGs were specific to one or two conditions at both post-exercise and recovery (Figure 6D), suggesting a disrupted transcriptional activation with histamine receptor blockade. Gene set enrichment analysis (GSEA) using the Hallmark database was then used to obtain insights into differential transcriptional activation of pathways between conditions at each time point (Figure 6E; Table S3). The largest effects were observed during the recovery phase for both H1 and H2 blockade, consistent with the temporal pattern of immune cell activation and infiltration.[61] As expected, multiple inflammation-related pathways were downregulated with H1 blockade (interferon response, tumor necrosis factor alpha [TNF-α] signaling, IL-6-STAT3 signaling, inflammatory response). Unexpected differences were found when comparing the effects of H1 versus H2 receptor blockade, however. Whereas H1 blockade induced a downregulation of inflammation-related pathways, these pathways were positively enriched with H2 blockade. Divergent effects for H1 versus H2 blockade were also uncovered for inferred transcription factor activities (e.g., *STAT3*, *STAT1*, *NFKB1*, and *TP53*), with, in general, larger effects with H1 blockade (Figure S6F). We then reanalyzed a previously published dataset on double blockade of H1 and H2 receptors with biopsy collection before and after aerobic exercise.[60] As reported previously, this double blockade induces a drastic downregulation of DEGs during recovery but not immediately after exercise (Figure S6G; Table S4). This is concomitant with a severely blunted enrichment of functional pathways (Figure S6H; Table S5), and more so compared with single blockade. These data illustrate that H1 blockade might be dominant during double blockade and that H1 and H2 receptors cooperate in driving exercise responses in skeletal muscle.

Finally, we applied our novel single-fiber transcriptomics workflow to the muscle biopsies collected with histamine receptor blockade (912 fibers for placebo, 929 fibers for H1 blockade, 969 fibers for H2 blockade). This allowed us to decipher if the histaminergic signaling that was initiated by exercise in the non-muscle cells would also result in distinct transcriptional responses in the myofibers. Pathway activity inference analysis on pseudobulked myofibers showed activation of multiple pathways (Figure 6F; Table S6). Overall, these responses were not different between placebo and both histamine blockade conditions, for example, for EGFR, MAPK, phosphatidylinositol 3-kinase (PI3K), and TGF-β. Notable exceptions during recovery were an upregulation of TNF-α and p53 activity in placebo but downregulation with H1 and especially H2 blockade. Altogether, histamine receptors appear to be synergistically involved in the transcriptional regulation of exercise responses, primarily mediated by non-muscle cells and especially in the inflammatory processes initiated upon homeostatic perturbations.

DISCUSSION

Most studies on skeletal muscle adaptations with exercise have focused on the bulk muscle response, therefore limiting the appreciation of the cellular diversity present in skeletal muscle. We have previously developed omics workflows on true single fibers to study fiber heterogeneity.[8,19] By comparing bulk muscle and myofiber-specific responses to exercise, we show the importance of a multicellular view of skeletal muscle as a tissue in which mononuclear cells interact with muscle cells to control muscle function. This is mainly demonstrated by the fact that the number of exercise-responsive genes in bulk muscle is an order of magnitude higher than that of only muscle fibers, showing that much of the activation and deactivation of transcriptional activity in response to exercise takes place outside the muscle fibers. As illustrated in the graphical abstract, this expands on more traditional textbook insights, stating that exercise induces metabolic perturbation in skeletal muscle fibers, which leads to signaling (e.g., mTOR and AMPK pathway) and transcriptional changes and eventually structural adaptations (e.g., hypertrophy and mitochondrial biogenesis) within those same muscle fibers.[62] We focused on several immune cell subtypes, which have previously been shown to be involved in muscle homeostasis,[63] and narrowed in on mast cells, a cell population that has previously remained unnoticed in skeletal muscle.

We specifically uncover a histamine-histamine receptor H1 (HRH1)/histamine receptor H2 (HRH2) axis, likely functioning via an intercellular network comprising mast cells, expressing HDC, and other myeloid and vascular cells, expressing histamine receptors. Histamine is selectively and locally released into the muscle interstitium during exercise in humans. Interstitial histidine levels were several orders of magnitude higher than histamine (10–200 μM versus 20–300 nM), suggesting that precursor (histidine) availability is unlikely to be a limiting factor for histamine production. This refutes an earlier hypothesis that the availability of histidine and alternative pathways to produce histidine from carnosine might be involved in the histaminergic signaling in skeletal muscle.[64] Furthermore, H1 and H2 receptor blockade induced divergent transcriptional responses, emphasizing the distinct role of the specific histamine receptors in the regulation of exercise responses, potentially via their expression on different immune and vascular cell subtypes. Follow-up work is needed to pinpoint how histamine receptor binding initiates transcriptional pathways, especially during the recovery phase after exercise. Overall, while the immediate histamine signaling is of a paracrine nature between non-muscle mononuclear cells, the long-term muscle adaptations related to aerobic capacity, insulin sensitivity, and microvascular function are also dependent on this histamine signaling cascade.[18]

A marked discovery in the histamine blockade experiment was the potent inhibition of glycogen resynthesis in the H1 receptor antagonist condition. The involvement of histamine in the regulation of metabolic recovery after exercise is puzzling since the receptors are not expressed on muscle cells, suggesting a role for intercellular signaling in the regulation of glucose homeostasis. The G protein-coupled histamine receptors have previously been linked to glucose metabolism in mice[47] and interstitial glucose concentrations in humans.[65] However, our data show that glucose processing and handling within myocytes is not affected. Glucose supply or transsarcolemmal transport are therefore more likely sites of action related to the impaired glycogen resynthesis.[53] We and others have shown that post-exercise perfusion of the muscle is blunted with histamine receptor blockade.[18,66] The perfusion in the muscle microcirculation could also be impaired with histamine receptor blockade,[52,65] which could be directly related to a lower glucose supply.[67] Also, a histamine-mediated regulatory role in macrophages/monocytes and neutrophils is a possible contributor to glucose control, as has been shown for IL-1-mediated GLUT4 translocation via neutrophils[54] or the importance of reactive oxygen species for muscle glucose uptake.[68] This could also be related to the impaired activation of p38 MAPK that we observed, which has been shown to be related to insulin-independent glucose uptake,[69] as also observed in *Rac1*-knockout (KO) muscle.[70] It also remains unclear if histamine receptors are involved in non-oxidative glucose disposal related to extracellular matrix proteoglycan remodeling.[71,72]

Overall, a major contribution of a small cell population such as mast cells is exciting since research on the role of mast cells in skeletal muscle is very scarce. A similar intercellular communication machinery, via muscle cells to stromal satellite cells, has previously been identified for the mitochondrial metabolite succinate.[33] These data further illustrate the importance of appreciating the large cell diversity and paracrine signaling within skeletal muscle to fully understand how muscle controls metabolic health[73] and adapts to exercise. A similar exercise-induced crosstalk with immune cells has recently been demonstrated with adipocytes in adipose tissue.[74] To more comprehensively profile immune cells in human skeletal muscle in the future, the use of different technologies (e.g., 5′- versus 3′-based sequencing) will be required. It is still unclear, however, how our cell crosstalk view relates to other signaling events, such as at the phosphoproteome or metabolome level, and if this is different between different types of exercise (e.g., high-intensity interval training, moderate-intensity continuous training, or resistance training).[5] Our profiling of novel potential intercellular communication networks using the CellChat and NicheNet algorithms identifies a profound complexity depending on the sender and receiver cell. These approaches help to identify novel communication networks. For example, we identified *S100A8/S100A9-TLR4* as a potential signaling network originating from myeloid cells. A recent paper indeed confirmed that this communication axis is important for the regulation of glucose homeostasis and could serve as a therapeutic target for type 1 diabetes.[75] Our results strongly suggest that modeling of intercellular communication patterns can discover new regulatory networks of interacting cells.

In conclusion, we uncover distinct exercise-induced transcriptional responses in mononuclear and muscle cells within the skeletal muscle microenvironment by integrating single-fiber and standard single-cell and bulk RNA-seq methodologies. Using this cellular deconstruction, we identify a histamine signaling cascade driving glycogen resynthesis and the transcriptional response to exercise. Our findings substantiate the intricate intercellular communication networks involved in the control of muscle homeostasis and remodeling.

Limitations of the study

We opted for an approach in humans, increasing the translational potential of our findings but hindering detailed mechanistic insights inherent to *in vitro* and/or rodent experiments. The latter types of experiments would help to further understand how mononuclear non-muscle cells communicate in the muscle microenvironment to control muscle glycogen resynthesis. Computational deconvolution approaches could be explored to profile the dynamics of infiltrating and resident cells during and after exercise, although these methods are inherently challenging due to the mixture of mononuclear non-muscle cells and multinucleated fibers in skeletal muscle. Follow-up experimental work will thus be required to gain additional insights into these dynamics. Our human exercise trial is also limited by not including a non-exercise control group, which allows for dissecting exercise-induced versus circadian effects on gene expression.[76] Furthermore, our relatively small sample sizes make it difficult to explore interindividual differences in exercise or histamine receptor blockade effects.

RESOURCE AVAILABILITY

Lead contact

Further information and requests for resources and reagents should be directed to and will be fulfilled by the lead contact, Wim Derave (wim.derave@ugent.be).

Materials availability

This study did not generate new, unique reagents.

Data and code availability

- Single-fiber and bulk muscle RNA-seq data have been deposited at the European Genome-phenome Archive (EGA), which is hosted by the EBI and the CRG, under accession number EGA: EGAD50000000612.
- The single-cell data are available for download at the Gene Expression Omnibus website (GEO Accession Code: GSE235143).
- High-resolution scans of all blots presented in the paper as well as an Excel file containing the values that were used to create all graphs in the paper have been included as Data S1—source data to this manuscript.
- This paper does not report the original code.
- All other data are available from the corresponding author on request.

ACKNOWLEDGMENTS

This work was generously funded by grants from the Research Foundation Flanders (FWO) (G080321N, 11B4220N, and V433222N to W.D., T.V.d.S., and T.V.d.S., respectively). All mass spectrometry experiments were performed using an UHPLC-MS/MS instrument part of the Ghent University MSsmall Expertise Centre for advanced mass spectrometry analysis of small organic molecules. Robin Browaeys (IRC VIB-UGent) is thanked for discussions on the CellChat and NicheNet analysis. Contributions from Kelly Lemeire (IRC VIB-UGent) and the VIB Bioimaging Core Ghent are appreciated for the RNAscope analysis. The technical assistance of Jens Jung Nielsen, Anneke Volkaert, Nicoline Resen Andersen, Betina Bolmgren, Thomas Ehlers, Jonas

Vandecauter, Ruben De Saegher, Karel Van Belleghem, Bart Wouters, Simon Meganck, Gill Callens, Laura Lecompte, Ruben Huysentruyt, Fauve Vanwelden, Thijs Oste, Nicklas Frisch, and Josephine Rol is greatly appreciated. Several illustrations were made with BioRender.com.

AUTHOR CONTRIBUTIONS

Conceptualization: T.V.d.S., A.V.d.L., J.R.H., P.M., E.A.R., L.G., Y.H., J.V., K.D.B., and W.D. Methodology: T.V.d.S., A.V.d.L., G.T., C.H., A.T.-E., M.U., J.S., S.D.B., L.D.W., P.V.E., P.M., L.G., Y.H., J.V., and W.D. Software: T.V.d.S., G.T., J.A., P.M., and J.V. Validation: T.V.d.S., A.V.d.L., C.H., A.T.-E., M.U., N.Y., J.A., S.D.B., P.M., J.V., and W.D. Formal analysis: T.V.d.S., A.V.d.L., G.T., A.T.-E., and J.A. Investigation: T.V.d.S., A.V.d.L., G.T., C.H., A.T.-E., M.U., E.L., J.S., N.Y., J.N., S.D.B., R.V.T., A.W., L.D.W., and L.G. Resources: P.V.E., S.C., J.R.H., P.M., E.A.R., L.G., Y.H., J.V., K.D.B., and W.D. Data curation: T.V.d.S., A.V.d.L., G.T., C.H., A.T.-E., M.U., E.L., N.Y., J.A., J.N., and S.D.B. Writing – original draft: T.V.d.S., A.V.d.L., and W.D. Writing – review and editing: T.V.d.S., A.V.d.L., G.T., C.H., A.T.-E., M.U., E.L., J.S., N.Y., J.A., J.N., S.D.B., R.V.T., A.W., L.D.W., P.V.E., S.C., J.R.H., P.M., E.A.R., L.G., Y.H., J.V., K.D.B., and W.D. Visualization: T.V.d.S., A.V.d.L., and G.T. Supervision: P.V.E., S.C., J.R.H., P.M., E.A.R., L.G., Y.H., J.V., K.D.B., and W.D. Project administration: T.V.d.S., A.V.d.L., G.T., C.H., L.G., Y.H., K.D.B., and W.D. Funding acquisition: T.V.d.S., P.V.E., S.C., P.M., E.A.R., L.G., Y.H., J.V., K.D.B., and W.D.

DECLARATION OF INTERESTS

The authors declare no competing interests.

STAR★METHODS

Detailed methods are provided in the online version of this paper and include the following:

- KEY RESOURCES TABLE
- EXPERIMENTAL MODEL AND STUDY PARTICIPANT DETAILS
  - Histamine blockade experiments
  - Histamine release experiments
- METHOD DETAILS
  - Histamine blockade experiments
  - Histamine release experiments
  - Biochemical analysis
  - Single-fiber RNA sequencing
  - Bulk muscle RNA sequencing
  - Single-cell RNA sequencing
  - Combined H1/H2 blockade RNA sequencing
  - Bioinformatics
- QUANTIFICATION AND STATISTICAL ANALYSIS

SUPPLEMENTAL INFORMATION

Supplemental information can be found online at https://doi.org/10.1016/j.cmet.2024.12.011.

Received: February 11, 2024
Revised: October 14, 2024
Accepted: December 18, 2024
Published: February 6, 2025

REFERENCES

1. Hawley, J.A., Hargreaves, M., Joyner, M.J., and Zierath, J.R. (2014). Integrative biology of exercise. Cell *159*, 738–749. https://doi.org/10.1016/j.cell.2014.10.029.
2. MacInnis, M.J., and Gibala, M.J. (2017). Physiological adaptations to interval training and the role of exercise intensity. J. Physiol. *595*, 2915–2930. https://doi.org/10.1113/JP273196.
3. Little, J.P., Safdar, A., Bishop, D., Tarnopolsky, M.A., and Gibala, M.J. (2011). An acute bout of high-intensity interval training increases the nuclear abundance of PGC-1α and activates mitochondrial biogenesis in human skeletal muscle. Am. J. Physiol. Regul. Integr. Comp. Physiol. *300*, R1303–R1310. https://doi.org/10.1152/ajpregu.00538.2010.
4. Perry, C.G.R., Lally, J., Holloway, G.P., Heigenhauser, G.J.F., Bonen, A., and Spriet, L.L. (2010). Repeated transient mRNA bursts precede increases in transcriptional and mitochondrial proteins during training in human skeletal muscle. J. Physiol. *588*, 4795–4810. https://doi.org/10.1113/jphysiol.2010.199448.
5. Blazev, R., Carl, C.S., Ng, Y.-K., Molendijk, J., Voldstedlund, C.T., Zhao, Y., Xiao, D., Kueh, A.J., Miotto, P.M., Haynes, V.R., et al. (2022). Phosphoproteomics of three exercise modalities identifies canonical signaling and C18ORF25 as an AMPK substrate regulating skeletal muscle function. Cell Metab. *34*, 1561–1577.e9. https://doi.org/10.1016/j.cmet.2022.07.003.
6. Li, V.L., He, Y., Contrepois, K., Liu, H., Kim, J.T., Wiggenhorn, A.L., Tanzo, J.T., Tung, A.S.-H., Lyu, X., Zushin, P.H., et al. (2022). An exercise-inducible metabolite that suppresses feeding and obesity. Nature *606*, 785–790. https://doi.org/10.1038/s41586-022-04828-5.
7. Schiaffino, S., and Reggiani, C. (2011). Fiber types in mammalian skeletal muscles. Physiol. Rev. *91*, 1447–1531. https://doi.org/10.1152/physrev.00031.2010.
8. Van der Stede, T., Van de Loock, A., Lievens, E., Yigit, N., Anckaert, J., Van Thienen, R., Weyns, A., Mestdagh, P., Vandesompele, J., and Derave, W. (2024). Transcriptomic signatures of human single skeletal muscle fibers in response to high-intensity interval exercise. Am. J. Physiol. Cell Physiol. *327*, C1249–C1262. https://doi.org/10.1152/ajpcell.00299.2024.
9. Deshmukh, A.S., Steenberg, D.E., Hostrup, M., Birk, J.B., Larsen, J.K., Santos, A., Kjøbsted, R., Hingst, J.R., Schéele, C.C., Murgia, M., et al. (2021). Deep muscle-proteomic analysis of freeze-dried human muscle biopsies reveals fiber type-specific adaptations to exercise training. Nat. Commun. *12*, 304. https://doi.org/10.1038/s41467-020-20556-8.
10. Pillon, N.J., Gabriel, B.M., Dollet, L., Smith, J.A.B., Sardón Puig, L., Botella, J., Bishop, D.J., Krook, A., and Zierath, J.R. (2020). Transcriptomic profiling of skeletal muscle adaptations to exercise and inactivity. Nat. Commun. *11*, 470. https://doi.org/10.1038/s41467-019-13869-w.
11. Coulis, G., Jaime, D., Guerrero-Juarez, C., Kastenschmidt, J.M., Farahat, P.K., Nguyen, Q., Pervolarakis, N., McLinden, K., Thurlow, L., Movahedi, S., et al. (2023). Single-cell and spatial transcriptomics identify a macrophage population associated with skeletal muscle fibrosis. Sci. Adv. *9*, eadd9984. https://doi.org/10.1126/sciadv.add9984.
12. De Micheli, A.J., Spector, J.A., Elemento, O., and Cosgrove, B.D. (2020). A reference single-cell transcriptomic atlas of human skeletal muscle tissue reveals bifurcated muscle stem cell populations. Skelet. Muscle *10*, 19. https://doi.org/10.1186/s13395-020-00236-3.
13. Fan, Z., Turiel, G., Ardicoglu, R., Ghobrial, M., Masschelein, E., Kocijan, T., Zhang, J., Tan, G., Fitzgerald, G., Gorski, T., et al. (2021). Exercise-induced angiogenesis is dependent on metabolically primed ATF3/4+ endothelial cells. Cell Metab. *33*, 1793–1807.e9. https://doi.org/10.1016/j.cmet.2021.07.015.
14. Zhang, J., Muri, J., Fitzgerald, G., Gorski, T., Gianni-Barrera, R., Masschelein, E., D'Hulst, G., Gilardoni, P., Turiel, G., Fan, Z., et al. (2020). Endothelial Lactate Controls Muscle Regeneration from Ischemia by Inducing M2-like Macrophage Polarization. Cell Metab. *31*, 1136–1153.e7. https://doi.org/10.1016/j.cmet.2020.05.004.
15. Song, Y., Yang, J., Li, T., Sun, X., Lin, R., He, Y., Sun, K., Han, J., Yang, G., Li, X., et al. (2023). CD34+ cell-derived fibroblast-macrophage cross-talk drives limb ischemia recovery through the OSM-ANGPTL signaling axis. Sci. Adv. *9*, eadd2632. https://doi.org/10.1126/sciadv.add2632.
16. Langston, P.K., Sun, Y., Ryback, B.A., Mueller, A.L., Spiegelman, B.M., Benoist, C., and Mathis, D. (2023). Regulatory T cells shield muscle mitochondria from interferon-γ-mediated damage to promote the beneficial

effects of exercise. Sci. Immunol. *8*, eadi5377. https://doi.org/10.1126/sciimmunol.adi5377.

17. Luttrell, M.J., and Halliwill, J.R. (2017). The Intriguing Role of Histamine in Exercise Responses. Exerc. Sport Sci. Rev. *45*, 16–23. https://doi.org/10.1249/JES.0000000000000093.
18. Van der Stede, T., Blancquaert, L., Stassen, F., Everaert, I., Van Thienen, R., Vervaet, C., Gliemann, L., Hellsten, Y., and Derave, W. (2021). Histamine H1 and H2 receptors are essential transducers of the integrative exercise training response in humans. Sci. Adv. *7*, eabf2856. https://doi.org/10.1126/sciadv.abf2856.
19. Moreno-Justicia, R., Van der Stede, T., Stocks, B., Laitila, J., Seaborne, R.A., de Loock, A.V., Lievens, E., Samodova, D., Marín-Arraiza, L., Dmytriyeva, O., et al. (2023). Human Skeletal Muscle Fiber Heterogeneity Beyond Myosin Heavy Chains. Preprint at bioRxiv. https://doi.org/10.1101/2023.09.07.556665.
20. Kelwick, R., Desanlis, I., Wheeler, G.N., and Edwards, D.R. (2015). The ADAMTS (A Disintegrin and Metalloproteinase with Thrombospondin motifs) family. Genome Biol. *16*, 113. https://doi.org/10.1186/s13059-015-0676-3.
21. Jones, R.G., Dimet-Wiley, A., Haghani, A., da Silva, F.M., Brightwell, C.R., Lim, S., Khadgi, S., Wen, Y., Dungan, C.M., Brooke, R.T., et al. (2023). A molecular signature defining exercise adaptation with ageing and in vivo partial reprogramming in skeletal muscle. J. Physiol. *601*, 763–782. https://doi.org/10.1113/JP283836.
22. Turiel, G., Desgeorges, T., Masschelein, E., Birrer, M., Zhang, J., Engelberger, S., and Bock, K.D. (2023). Single cell compendium of the muscle microenvironment in peripheral artery disease reveals capillary endothelial heterogeneity and activation of resident macrophages. Preprint at bioRxiv. https://doi.org/10.1101/2023.06.21.545899.
23. Armingol, E., Baghdassarian, H.M., and Lewis, N.E. (2024). The diversification of methods for studying cell-cell interactions and communication. Nat. Rev. Genet. *25*, 381–400. https://doi.org/10.1038/s41576-023-00685-8.
24. Murphy, R.M., Watt, M.J., and Febbraio, M.A. (2020). Metabolic communication during exercise. Nat. Metab. *2*, 805–816. https://doi.org/10.1038/s42255-020-0258-x.
25. Leuchtmann, A.B., Adak, V., Dilbaz, S., and Handschin, C. (2021). The Role of the Skeletal Muscle Secretome in Mediating Endurance and Resistance Training Adaptations. Front. Physiol. *12*, 709807. https://doi.org/10.3389/fphys.2021.709807.
26. Chen, X., and Li, Y. (2009). Role of matrix metalloproteinases in skeletal muscle: migration, differentiation, regeneration and fibrosis. Cell Adh. Migr. *3*, 337–341. https://doi.org/10.4161/cam.3.4.9338.
27. Findeisen, M., Allen, T.L., Henstridge, D.C., Kammoun, H., Brandon, A.E., Baggio, L.L., Watt, K.I., Pal, M., Cron, L., Estevez, E., et al. (2019). Treatment of type 2 diabetes with the designer cytokine IC7Fc. Nature *574*, 63–68. https://doi.org/10.1038/s41586-019-1601-9.
28. Vinel, C., Lukjanenko, L., Batut, A., Deleruyelle, S., Pradère, J.-P., Le Gonidec, S., Dortignac, A., Geoffre, N., Pereira, O., Karaz, S., et al. (2018). The exerkine apelin reverses age-associated sarcopenia. Nat. Med. *24*, 1360–1371. https://doi.org/10.1038/s41591-018-0131-6.
29. Norheim, F., Raastad, T., Thiede, B., Rustan, A.C., Drevon, C.A., and Haugen, F. (2011). Proteomic identification of secreted proteins from human skeletal muscle cells and expression in response to strength training. Am. J. Physiol. Endocrinol. Metab. *301*, E1013–E1021. https://doi.org/10.1152/ajpendo.00326.2011.
30. Matthews, V.B., Aström, M.B., Chan, M.H.S., Bruce, C.R., Krabbe, K.S., Prelovsek, O., Akerström, T., Yfanti, C., Broholm, C., Mortensen, O.H., et al. (2009). Brain-derived neurotrophic factor is produced by skeletal muscle cells in response to contraction and enhances fat oxidation via activation of AMP-activated protein kinase. Diabetologia *52*, 1409–1418. https://doi.org/10.1007/s00125-009-1364-1.
31. Seldin, M.M., Lei, X., Tan, S.Y., Stanson, K.P., Wei, Z., and Wong, G.W. (2013). Skeletal muscle-derived myonectin activates the mammalian target of rapamycin (mTOR) pathway to suppress autophagy in liver. J. Biol. Chem. *288*, 36073–36082. https://doi.org/10.1074/jbc.M113.500736.
32. Nieman, D.C., Davis, J.M., Henson, D.A., Walberg-Rankin, J., Shute, M., Dumke, C.L., Utter, A.C., Vinci, D.M., Carson, J.A., Brown, A., et al. (2003). Carbohydrate ingestion influences skeletal muscle cytokine mRNA and plasma cytokine levels after a 3-h run. J. Appl. Physiol. (1985) *94*, 1917–1925. https://doi.org/10.1152/japplphysiol.01130.2002.
33. Reddy, A., Bozi, L.H.M., Yaghi, O.K., Mills, E.L., Xiao, H., Nicholson, H.E., Paschini, M., Paulo, J.A., Garrity, R., Laznik-Bogoslavski, D., et al. (2020). pH-Gated Succinate Secretion Regulates Muscle Remodeling in Response to Exercise. Cell *183*, 62–75.e17. https://doi.org/10.1016/j.cell.2020.08.039.
34. Abdelmoez, A.M., Dmytriyeva, O., Zurke, Y.-X., Trauelsen, M., Marica, A.A., Savikj, M., Smith, J.A.B., Monaco, C., Schwartz, T.W., Krook, A., et al. (2023). Cell selectivity in succinate receptor SUCNR1/GPR91 signaling in skeletal muscle. Am. J. Physiol. Endocrinol. Metab. *324*, E289–E298. https://doi.org/10.1152/ajpendo.00009.2023.
35. Wei, W., Riley, N.M., Lyu, X., Shen, X., Guo, J., Raun, S.H., Zhao, M., Moya-Garzon, M.D., Basu, H., Sheng-Hwa Tung, A., et al. (2023). Organism-wide, cell-type-specific secretome mapping of exercise training in mice. Cell Metab. *35*, 1261–1279.e11. https://doi.org/10.1016/j.cmet.2023.04.011.
36. Browaeys, R., Saelens, W., and Saeys, Y. (2020). NicheNet: modeling intercellular communication by linking ligands to target genes. Nat. Methods *17*, 159–162. https://doi.org/10.1038/s41592-019-0667-5.
37. Langston, P.K., and Mathis, D. (2024). Immunological regulation of skeletal muscle adaptation to exercise. Cell Metab. *36*, 1175–1183. https://doi.org/10.1016/j.cmet.2024.04.001.
38. Delaney, K., Kasprzycka, P., Ciemerych, M.A., and Zimowska, M. (2017). The role of TGF-β1 during skeletal muscle regeneration. Cell Biol. Int. *41*, 706–715. https://doi.org/10.1002/cbin.10725.
39. Kedlian, V.R., Wang, Y., Liu, T., Chen, X., Bolt, L., Tudor, C., Shen, Z., Fasouli, E.S., Prigmore, E., Kleshchevnikov, V., et al. (2024). Human skeletal muscle aging atlas. Nat. Aging *4*, 727–744. https://doi.org/10.1038/s43587-024-00613-3.
40. Lai, Y., Ramírez-Pardo, I., Isern, J., An, J., Perdiguero, E., Serrano, A.L., Li, J., García-Domínguez, E., Segalés, J., Guo, P., et al. (2024). Multimodal cell atlas of the ageing human skeletal muscle. Nature *629*, 154–164. https://doi.org/10.1038/s41586-024-07348-6.
41. Rubenstein, A.B., Smith, G.R., Raue, U., Begue, G., Minchev, K., Ruf-Zamojski, F., Nair, V.D., Wang, X., Zhou, L., Zaslavsky, E., et al. (2020). Single-cell transcriptional profiles in human skeletal muscle. Sci. Rep. *10*, 229. https://doi.org/10.1038/s41598-019-57110-6.
42. Jin, S., Guerrero-Juarez, C.F., Zhang, L., Chang, I., Ramos, R., Kuan, C.-H., Myung, P., Plikus, M.V., and Nie, Q. (2021). Inference and analysis of cell-cell communication using CellChat. Nat. Commun. *12*, 1088. https://doi.org/10.1038/s41467-021-21246-9.
43. Kim, M.J., Febbraro, D., Farkona, S., Gillmore, T., Son, J.E., Regeenes, R., Chang, H.H., Pollock-Tahiri, E., Yang, J., Park, Y.J., et al. (2021). Distinct roles of UVRAG and EGFR signaling in skeletal muscle homeostasis. Mol. Metab. *47*, 101185. https://doi.org/10.1016/j.molmet.2021.101185.
44. Metcalfe, D.D., Baram, D., and Mekori, Y.A. (1997). Mast cells. Physiol. Rev. *77*, 1033–1079. https://doi.org/10.1152/physrev.1997.77.4.1033.
45. Panula, P., Chazot, P.L., Cowart, M., Gutzmer, R., Leurs, R., Liu, W.L.S., Stark, H., Thurmond, R.L., and Haas, H.L. (2015). International Union of Basic and Clinical Pharmacology. XCVIII. Histamine Receptors. Pharmacol. Rev. *67*, 601–655. https://doi.org/10.1124/pr.114.010249.
46. Endo, Y., Tabata, T., Kuroda, H., Tadano, T., Matsushima, K., and Watanabe, M. (1998). Induction of histidine decarboxylase in skeletal muscle in mice by electrical stimulation, prolonged walking and interleukin-1. J. Physiol. *509*, 587–598. https://doi.org/10.1111/j.1469-7793.1998.587bn.x.
47. Niijima-Yaoita, F., Tsuchiya, M., Ohtsu, H., Yanai, K., Sugawara, S., Endo, Y., and Tadano, T. (2012). Roles of histamine in exercise-induced

fatigue: favouring endurance and protecting against exhaustion. Biol. Pharm. Bull. *35*, 91–97. https://doi.org/10.1248/bpb.35.91.

48. Savany, A., and Cronenberger, L. (1982). Properties of histidine decarboxylase from rat gastric mucosa. Eur. J. Biochem. *123*, 593–599. https://doi.org/10.1111/j.1432-1033.1982.tb06574.x.

49. Mangum, J.E., Needham, K.W., Sieck, D.C., Ely, M.R., Larson, E.A., Peck, M.C., Minson, C.T., and Halliwill, J.R. (2022). The effect of local passive heating on skeletal muscle histamine concentration: implications for exercise-induced histamine release. J. Appl. Physiol. (1985) *132*, 367–374. https://doi.org/10.1152/japplphysiol.00740.2021.

50. Jeong, H.J., Moon, P.D., Kim, S.J., Seo, J.U., Kang, T.H., Kim, J.J., Kang, I.C., Um, J.Y., Kim, H.M., and Hong, S.H. (2009). Activation of hypoxia-inducible factor-1 regulates human histidine decarboxylase expression. Cell. Mol. Life Sci. *66*, 1309–1319. https://doi.org/10.1007/s00018-009-9001-1.

51. Anrep, G.V., and Barsoum, G.S. (1935). Appearance of histamine in the venous blood during muscular contraction. J. Physiol. *85*, 409–420. https://doi.org/10.1113/jphysiol.1935.sp003328.

52. Romero, S.A., McCord, J.L., Ely, M.R., Sieck, D.C., Buck, T.M., Luttrell, M.J., MacLean, D.A., and Halliwill, J.R. (2017). Mast cell degranulation and de novo histamine formation contribute to sustained postexercise vasodilation in humans. J. Appl. Physiol. (1985) *122*, 603–610. https://doi.org/10.1152/japplphysiol.00633.2016.

53. Richter, E.A., and Hargreaves, M. (2013). Exercise, GLUT4, and skeletal muscle glucose uptake. Physiol. Rev. *93*, 993–1017. https://doi.org/10.1152/physrev.00038.2012.

54. Tsuchiya, M., Sekiai, S., Hatakeyama, H., Koide, M., Chaweewannakorn, C., Yaoita, F., Tan-No, K., Sasaki, K., Watanabe, M., Sugawara, S., et al. (2018). Neutrophils Provide a Favorable IL-1-Mediated Immunometabolic Niche that Primes GLUT4 Translocation and Performance in Skeletal Muscles. Cell Rep. *23*, 2354–2364. https://doi.org/10.1016/j.celrep.2018.04.067.

55. Sylow, L., Tokarz, V.L., Richter, E.A., and Klip, A. (2021). The many actions of insulin in skeletal muscle, the paramount tissue determining glycemia. Cell Metab. *33*, 758–780. https://doi.org/10.1016/j.cmet.2021.03.020.

56. Thong, F.S.L., Derave, W., Urso, B., Kiens, B., and Richter, E.A. (2003). Prior exercise increases basal and insulin-induced p38 mitogen-activated protein kinase phosphorylation in human skeletal muscle. J. Appl. Physiol. (1985) *94*, 2337–2341. https://doi.org/10.1152/japplphysiol.00036.2003.

57. Kramer, H.F., and Goodyear, L.J. (2007). Exercise, MAPK, and NF-kappaB signaling in skeletal muscle. J. Appl. Physiol. (1985) *103*, 388–395. https://doi.org/10.1152/japplphysiol.00085.2007.

58. Brennan, C.M., Emerson, C.P., Owens, J., and Christoforou, N. (2021). p38 MAPKs - roles in skeletal muscle physiology, disease mechanisms, and as potential therapeutic targets. JCI Insight *6*, e149915. https://doi.org/10.1172/jci.insight.149915.

59. Trenerry, M.K., Carey, K.A., Ward, A.C., and Cameron-Smith, D. (2007). STAT3 signaling is activated in human skeletal muscle following acute resistance exercise. J. Appl. Physiol. (1985) *102*, 1483–1489. https://doi.org/10.1152/japplphysiol.01147.2006.

60. Romero, S.A., Hocker, A.D., Mangum, J.E., Luttrell, M.J., Turnbull, D.W., Struck, A.J., Ely, M.R., Sieck, D.C., Dreyer, H.C., and Halliwill, J.R. (2016). Evidence of a broad histamine footprint on the human exercise transcriptome. J. Physiol. *594*, 5009–5023. https://doi.org/10.1113/JP272177.

61. Pillon, N.J., Smith, J.A.B., Alm, P.S., Chibalin, A.V., Alhusen, J., Arner, E., Carninci, P., Fritz, T., Otten, J., Olsson, T., et al. (2022). Distinctive exercise-induced inflammatory response and exerkine induction in skeletal muscle of people with type 2 diabetes. Sci. Adv. *8*, eabo3192. https://doi.org/10.1126/sciadv.abo3192.

62. Egan, B., and Sharples, A.P. (2023). Molecular responses to acute exercise and their relevance for adaptations in skeletal muscle to exercise training. Physiol. Rev. *103*, 2057–2170. https://doi.org/10.1152/physrev.00054.2021.

63. Pillon, N.J., Bilan, P.J., Fink, L.N., and Klip, A. (2013). Cross-talk between skeletal muscle and immune cells: muscle-derived mediators and metabolic implications. Am. J. Physiol. Endocrinol. Metab. *304*, E453–E465. https://doi.org/10.1152/ajpendo.00553.2012.

64. Boldyrev, A.A., Aldini, G., and Derave, W. (2013). Physiology and pathophysiology of carnosine. Physiol. Rev. *93*, 1803–1845. https://doi.org/10.1152/physrev.00039.2012.

65. Pellinger, T.K., Simmons, G.H., Maclean, D.A., and Halliwill, J.R. (2010). Local histamine H(1-) and H(2)-receptor blockade reduces postexercise skeletal muscle interstitial glucose concentrations in humans. Appl. Physiol. Nutr. Metab. *35*, 617–626. https://doi.org/10.1139/H10-055.

66. McCord, J.L., and Halliwill, J.R. (2006). H1 and H2 receptors mediate postexercise hyperemia in sedentary and endurance exercise-trained men and women. J. Appl. Physiol. (1985) *101*, 1693–1701. https://doi.org/10.1152/japplphysiol.00441.2006.

67. Sjøberg, K.A., Frøsig, C., Kjøbsted, R., Sylow, L., Kleinert, M., Betik, A.C., Shaw, C.S., Kiens, B., Wojtaszewski, J.F.P., Rattigan, S., et al. (2017). Exercise Increases Human Skeletal Muscle Insulin Sensitivity via Coordinated Increases in Microvascular Perfusion and Molecular Signaling. Diabetes *66*, 1501–1510. https://doi.org/10.2337/db16-1327.

68. Henríquez-Olguin, C., Knudsen, J.R., Raun, S.H., Li, Z., Dalbram, E., Treebak, J.T., Sylow, L., Holmdahl, R., Richter, E.A., Jaimovich, E., et al. (2019). Cytosolic ROS production by NADPH oxidase 2 regulates muscle glucose uptake during exercise. Nat. Commun. *10*, 4623. https://doi.org/10.1038/s41467-019-12523-9.

69. Bengal, E., Aviram, S., and Hayek, T. (2020). p38 MAPK in Glucose Metabolism of Skeletal Muscle: Beneficial or Harmful? Int. J. Mol. Sci. *21*, 6480. https://doi.org/10.3390/ijms21186480.

70. Raun, S.H., Henriquez-Olguín, C., Frank, E., Knudsen, J.R., Ali, M.S., Andersen, N.R., Møller, L.L.V., Davey, J., Qian, H., Coelho, A., et al. (2023). The Rho GTPase Rac1 mediates exercise training adaptations. Preprint at bioRxiv. https://doi.org/10.1101/2023.10.08.561442.

71. Hyldahl, R.D., Chen, T.C., and Nosaka, K. (2017). Mechanisms and Mediators of the Skeletal Muscle Repeated Bout Effect. Exerc. Sport Sci. Rev. *45*, 24–33. https://doi.org/10.1249/JES.0000000000000095.

72. Nascimento, E.B.M., Hangelbroek, R.W.J., Hooiveld, G.J.E.J., Hoeks, J., Van Marken Lichtenbelt, W.D., Hesselink, M.H.C., Schrauwen, P., and Kersten, S. (2020). Comparative transcriptome analysis of human skeletal muscle in response to cold acclimation and exercise training in human volunteers. BMC Med. Genomics *13*, 124. https://doi.org/10.1186/s12920-020-00784-z.

73. Zhang, J., Sjøberg, K.A., Gong, S., Wang, T., Li, F., Kuo, A., Durot, S., Majcher, A., Ardicoglu, R., Desgeorges, T., et al. (2024). Endothelial metabolic control of insulin sensitivity through resident macrophages. Cell Metab. *36*, 2383–2401.e9. https://doi.org/10.1016/j.cmet.2024.08.008.

74. Dollet, L., Lundell, L.S., Chibalin, A.V., Pendergrast, L.A., Pillon, N.J., Lansbury, E.L., Elmastas, M., Frendo-Cumbo, S., Jalkanen, J., de Castro Barbosa, T., et al. (2024). Exercise-induced crosstalk between immune cells and adipocytes in humans: Role of oncostatin-M. Cell Rep. Med. *5*, 101348. https://doi.org/10.1016/j.xcrm.2023.101348.

75. Ursino, G., Lucibello, G., Teixeira, P.D.S., Höfler, A., Veyrat-Durebex, C., Odouard, S., Visentin, F., Galgano, L., Somm, E., Vianna, C.R., et al. (2024). S100A9 exerts insulin-independent antidiabetic and anti-inflammatory effects. Sci. Adv. *10*, eadj4686. https://doi.org/10.1126/sciadv.adj4686.

76. Perrin, L., Loizides-Mangold, U., Chanon, S., Gobet, C., Hulo, N., Isenegger, L., Weger, B.D., Migliavacca, E., Charpagne, A., Betts, J.A., et al. (2018). Transcriptomic analyses reveal rhythmic and CLOCK-driven pathways in human skeletal muscle. eLife *7*, e34114. https://doi.org/10.7554/eLife.34114.

77. Gliemann, L., Rytter, N., Piil, P., Nilton, J., Lind, T., Nyberg, M., Cocks, M., and Hellsten, Y. (2018). The Endothelial Mechanotransduction Protein Platelet Endothelial Cell Adhesion Molecule-1 Is Influenced by Aging and Exercise Training in Human Skeletal Muscle. Front. Physiol. *9*, 1807. https://doi.org/10.3389/fphys.2018.01807.

78. Van der Stede, T., Spaas, J., de Jager, S., De Brandt, J., Hansen, C., Stautemas, J., Vercammen, B., De Baere, S., Croubels, S., Van Assche, C.-H., et al. (2023). Extensive profiling of histidine-containing dipeptides reveals species- and tissue-specific distribution and metabolism in mice, rats, and humans. Acta Physiol. (Oxf) *239*, e14020. https://doi.org/10.1111/apha.14020.

79. Gliemann, L., Rytter, N., Tamariz-Ellemann, A., Egelund, J., Brandt, N., Carter, H.H., and Hellsten, Y. (2020). Lifelong Physical Activity Determines Vascular Function in Late Postmenopausal Women. Med. Sci. Sports Exerc. *52*, 627–636. https://doi.org/10.1249/MSS.0000000000002180.

80. Lockwood, J.M., Wilkins, B.W., and Halliwill, J.R. (2005). H1 receptor-mediated vasodilatation contributes to postexercise hypotension. J. Physiol. *563*, 633–642. https://doi.org/10.1113/jphysiol.2004.080325.

81. McCord, J.L., Beasley, J.M., and Halliwill, J.R. (2006). H2-receptor-mediated vasodilation contributes to postexercise hypotension. J. Appl. Physiol. (1985) *100*, 67–75. https://doi.org/10.1152/japplphysiol.00959.2005.

82. Russell, T., Stoltz, M., and Weir, S. (1998). Pharmacokinetics, pharmacodynamics, and tolerance of single- and multiple-dose fexofenadine hydrochloride in healthy male volunteers. Clin. Pharmacol. Ther. *64*, 612–621. https://doi.org/10.1016/S0009-9236(98)90052-2.

83. Kroemer, H., and Klotz, U. (1987). Pharmacokinetics of famotidine in man. Int. J. Clin. Pharmacol. Ther. Toxicol. *25*, 458–463.

84. Bergstrom, J. (1975). Percutaneous needle biopsy of skeletal muscle in physiological and clinical research. Scand. J. Clin. Lab. Invest. *35*, 609–616. https://doi.org/10.3109/00365517509095787.

85. Lowry, O., and Passonneau, J. (1972). A Flexible System of Enzymatic Analysis. In A Flexible System of Enzymatic Analysis (Academic Press), pp. 237–249. https://doi.org/10.1016/B978-0-12-457950-7.X5001-3.

86. Hao, Y., Hao, S., Andersen-Nissen, E., Mauck, W.M., Zheng, S., Butler, A., Lee, M.J., Wilk, A.J., Darby, C., Zager, M., et al. (2021). Integrated analysis of multimodal single-cell data. Cell *184*, 3573–3587.e29. https://doi.org/10.1016/j.cell.2021.04.048.

87. Choudhary, S., and Satija, R. (2022). Comparison and evaluation of statistical error models for scRNA-seq. Genome Biol. *23*, 27. https://doi.org/10.1186/s13059-021-02584-9.

88. Squair, J.W., Gautier, M., Kathe, C., Anderson, M.A., James, N.D., Hutson, T.H., Hudelle, R., Qaiser, T., Matson, K.J.E., Barraud, Q., et al. (2021). Confronting false discoveries in single-cell differential expression. Nat. Commun. *12*, 5692. https://doi.org/10.1038/s41467-021-25960-2.

89. Xiao, Y., Hsiao, T.-H., Suresh, U., Chen, H.-I.H., Wu, X., Wolf, S.E., and Chen, Y. (2014). A novel significance score for gene selection and ranking. Bioinformatics *30*, 801–807. https://doi.org/10.1093/bioinformatics/btr671.

90. Hostrup, M., Lemminger, A.K., Stocks, B., Gonzalez-Franquesa, A., Larsen, J.K., Quesada, J.P., Thomassen, M., Weinert, B.T., Bangsbo, J., and Deshmukh, A.S. (2022). High-intensity interval training remodels the proteome and acetylome of human skeletal muscle. eLife *11*, e69802. https://doi.org/10.7554/eLife.69802.

91. Jin, S., Plikus, M.V., and Nie, Q. (2024). CellChat for systematic analysis of cell-cell communication from single-cell and spatially resolved transcriptomics. Nat. Protoc. *20*. https://doi.org/10.1038/s41596-024-01045-4.

STAR★METHODS

KEY RESOURCES TABLE

REAGENT or RESOURCE	SOURCE	IDENTIFIER
Antibodies		
Anti-human pGS 2+2a	Custom made Dr. David Grahame Hardie	N/A
Anti-human pGS 3a+3b	Custom made Dr. David Grahame Hardie	N/A
Anti-human GS total	Custom made Dr. Oluf Pedersen	N/A
Anti-human pAkt Ser473	Cell Signaling	Cat#9271; RRID:AB_329825
Anti-human pAkt Thr308	Cell Signaling	Cat#9275; RRID:AB_329828
Anti-human Akt total	Cell Signaling	Cat#3063; RRID:AB_2225186
Anti-human pTBC1D1 Ser237	Millipore	Cat#07-2268; RRID:AB_11211221
Anti-human TBC1D1 total	Abcam	Cat#229504; RRID:AB_2814949
Anti-human pTBCD1D4 Thr642	Cell Signaling	Cat#8881; RRID:AB_2651042
Anti-human pTBCD1D4 Ser588	Cell Signaling	Cat#8730; RRID:AB_10860251
Anti-human TBC1D4 total	Abcam	Cat#189890; RRID:AB_2818964
Anti-human pAMPK Thr172	Cell Signaling	Cat#2531; RRID:AB_330330
Anti-human AMPKα2 total	Abcam	Cat#3760; RRID:AB_304055
Anti-human pACC Ser80	Cell Signaling	Cat#3661; RRID:AB_330337
Anti-human ACC total	Dako	Cat#P0397
Anti-human p-p38 MAPK Thr180/Tyr182	Cell Signaling	Cat#9211; RRID:AB_331641
Anti-human p38 MAPK total	Cell Signaling	Cat#9212; RRID:AB_330713
Anti-human pERK1/2 Thr202 / Tyr204	Cell Signaling	Cat#9101; RRID:AB_331646
Anti-human ERK1/2 total	Cell Signaling	Cat#9102; RRID:AB_330744
Anti-human p-p65 NFκβ Ser536	Cell Signaling	Cat#3033; RRID:AB_331284
Anti-human p65 NFκβ total	Cell Signaling	Cat#4764; RRID:AB_823578
Anti-human pSTAT3 Tyr705	Cell Signaling	Cat#9138; RRID:AB_331262
HRP Donkey anti-rabbit	Jackson Immuno Research	Cat#711-035-152; RRID:AB_10015282
HRP Donkey anti-mouse	Jackson Immuno Research	Cat#715-035-151; RRID:AB_2340771
Human HRH1 RNAscope probe	Advanced Cell Diagnostics	Cat#416501-C3
Human HRH2 RNAscope probe	Advanced Cell Diagnostics	Cat#416511-C2
Human HDC RNAscope probe	Advanced Cell Diagnostics	Cat#311441
Human TPSB2 RNAscope probe	Advanced Cell Diagnostics	Cat#577161-C2
Human FOLR2 RNAscope probe	Advanced Cell Diagnostics	Cat#1286201-C1
Human CD1C RNAscope probe	Advanced Cell Diagnostics	Cat#514761
Human SLC11A1 RNAscope probe	Advanced Cell Diagnostics	Cat#543541
Human PDGFRA RNAscope probe	Advanced Cell Diagnostics	Cat#604481
Human PECAM1 RNAscope probe	Advanced Cell Diagnostics	Cat#487381
Human ACTA2 RNAscope probe	Advanced Cell Diagnostics	Cat#444771
Wheat germ agglutinin	Biotium	Cat#290059
DAPI stain	Thermo Fisher Scientific	Cat#D1306
Chemicals, peptides, and recombinant proteins		
RNAlater	Thermo Fisher Scientific	Cat#AM7021
glucose D-[3-3H]	PerkinElmer	Cat#NET331A
Ringer-acetate	Fresenius Kabi	Cat#468932
Histamine	Merck	Cat#59964

(*Continued on next page*)

Continued

REAGENT or RESOURCE	SOURCE	IDENTIFIER
4-imidazole acetic acid hydrochloride	Merck	Cat#219991
L-histidine	Merck	Cat#H8000
histamine-α,α,β,β-d4 dihydrochloride	Merck	Cat#762962
N-methylhistamine	Sanbio	Cat#19516-10
1-methyl-4-imidazole aceKc acid hydrochloride	Sanbio	Cat#18815-10
Critical commercial assays		
Pierce protein assay kit	Thermo Fisher Scientific	Cat#23225
Pierce Reversible Protein Stain Kit for PVDF membranes	Thermo Fisher Scientific	Cat#24585
Immobilon Forte Western HRP substrate	Millipore	Cat#WBLUF0020
RNAscope multiplex fluorescent reagent kit v2	Advanced Cell Diagnostics	Cat#323285
SingleShot Cell Lysis kit	Bio-Rad	Cat#1725080
QuantSeq-Pool 3' mRNA-Seq library prep kit	Lexogen	Cat#139.96
High sensitivity small DNA Fragment Analysis kit	Agilent Technologies	Cat#DNF-477-0500
NovaSeq 6000 S2 Reagent Kit v1.5 (200 cycles)	Illumina	Cat#20028315
NovaSeq 6000 S2 Reagent Kit v1.5 (100 cycles)	Illumina	Cat#20028316
miRNeasy Mini kit	Qiagen	Cat#217004
HL-dsDNase kit	ArcticZymes	Cat#70800
SMARTer Stranded Total RNA-Seq Kit (v3 - Pico Input 891 Mammalian)	Takara Bio	Cat#634487
SMARTer RNA Unique Dual Index Kit – 96U Set A	Takara Bio	Cat#634452
SMARTer RNA Unique Dual Index Kit – 96U Set B	Takara Bio	Cat#634457
Deposited data		
Bulk muscle RNA-seq data with single histamine receptor blockade	This paper	EGAD50000000612
Single-fiber RNA-seq data	This paper	EGAD50000000612
Single-cell RNA-seq data	Turiel et al.[22]	GSE235143
Bulk muscle RNA-seq data with double histamine receptor blockade	Romero et al.[60]	GSE71972
Data S1 – Source data	This paper	N/A
Software and algorithms		
R v. 4.2.3	CRAN	https://www.r-project.org
QuPath v. 0.5.1	QuPath	https://qupath.github.io
ImageLab v. 6.1	Bio-Rad	https://www.bio-rad.com/en-be/product/image-lab-software?ID=KRE6P5E8Z
MassLynx v. 4.2	Waters	https://www.waters.com/nextgen/en/products/informatics-and-software/mass-spectrometry-software/masslynx-mass-spectrometry-software.html?srsltid=AfmBOoo1MHb0IwAWzdQXWenTttxdBey79-cVBf-UtKPRTbl66nN7OlBw
QuantSeq Pool analysis pipeline	Lexogen	https://github.com/Lexogen-Tools/quantseqpool_analysis
Illustrator v. 29.1	Adobe	https://www.adobe.com/be_en/products/illustrator.html
Other		
Cyclus 2 ergometer	RBM Elektronik-automation	https://www.cyclus2.com/en/
Excalibur Sport ergometer	Lode	https://lode-ergometry.com/product/excalibur-sport/
Fexofenadine	Telfast	N/A
Famotidine	Aurobindo Pharma	N/A
Microdialysis catheter (20 kDa)	MDialysis AB	#8010514

EXPERIMENTAL MODEL AND STUDY PARTICIPANT DETAILS

Histamine blockade experiments

Fourteen (12M, 2F) healthy adults participated in the study. Participants received oral and written information about all study procedures including possible risks associated with participation. After giving written informed consent, participants were medically screened before final inclusion. All participants were non-smoking, between the age of 22 and 42 years, moderately physically active and free of chronic diseases or allergy symptoms with no intake of medication or food supplements. General characteristics have been described before.[19] Exercise-related characteristics include maximal heart rate (192 ± 9 beats per minute), maximal oxygen uptake (49.7 ± 9.1 $mL \cdot min^{-1} \cdot kg^{-1}$) and power output at peak power (336 ± 48 W), gas exchange threshold (128 ± 20 W) and respiratory compensation point (198 ± 26 W).

Histamine release experiments

For the first microdialysis experiment, participants consisted of two groups: young (n=4) and old (n=8) healthy men, as described before.[77,78] Seven healthy, young men were recruited for the second experiment consisting of microdialysis and arterial-venous sampling.[78] Post-menopausal women were recruited for the second arterial-venous sampling experiment.[79]

METHOD DETAILS

Histamine blockade experiments

Study design

This study conforms with the 2013 standards set by the Declaration of Helsinki, was approved by the Ethical Committee of Ghent University Hospital, Belgium (BC-10237) and is registered in ClinicalTrials.gov (NCT05131555). Testing was performed in a temperature- and humidity-controlled room (18 °C and 50%, respectively) at the Sports Science Laboratory Jacques Rogge at Ghent University. Cycling testing and exercise was performed on calibrated cycling ergometers, Cyclus2 (RBM Elektronik-automation, Leipzig, Germany) or Excalibur Sport (Lode, Groningen, The Netherlands), and preferred cycling cadence was recorded during the first testing visit and replicated during the following visits. Participants abstained from caffeine, exercise, and alcohol for 24 and 48 h prior to each pre-experimental and experimental day, respectively. All tests were performed at the same time of day to minimize circadian differences.

Pre-experimental days

In a cross-over, double-blind (researcher and participants), randomized study design, participants attended the laboratory on 5 occasions. On a first test day, anthropometrical data (height and body weight) were collected and a maximal incremental cycling test was performed from which maximal performance (maximal oxygen uptake and peak power output) and submaximal ventilatory thresholds (Gas Exchange Threshold, GET, and Respiratory Compensation Point, RCP) were derived for the following experimental days. On the second test day (2-3 days later), a familiarisation training was performed to ensure adequate exercise intensities for the cycling interval training used on the actual experimental days. The intensity of the interval bouts was increased or decreased by ± 10 W if deemed necessary. Food intake was similar 24 h prior to the maximal cycling test and familiarisation session, and this familiarisation session was planned 4-5 days before the actual experimental days.

Maximal incremental cycling test

The test started by cycling for 6 min at 100/70 W (male/female), followed by 2 min of rest, and a 4-min warm-up at 50/40 W. Then, work rate increased continuously by 25/20 W every minute until volitional exhaustion despite strong verbal encouragement. Specific details on measurement instruments and methodology of ventilatory threshold determination have been described previously.[18] Analysis was performed in RStudio using the *whippr* package (v. 0.1.2).

Experimental days

Participants reported to the laboratory for three parallel experimental days (placebo, H1 receptor blockade and H2 receptor blockade, in randomized order), separated by 14 days. To ensure similar starting muscle glycogen concentrations on each experimental day, food intake was standardized for 48 h before each day by providing ready-to-eat meals, consisting of approximately 41.4 kcal/kg body weight (BW), 5.1 g/kg BW carbohydrates, 1.4 g/kg BW protein and 1.6 g/kg BW fat per day. On the day of the experiment, participants consumed a standardized breakfast consisting of white bread, strawberry jam and apple juice (1.5 g/kg BW carbohydrates). Thirty minutes later, they ingested ~150 mL of water and capsules containing either H1- or H2 receptor blockers or placebo. Thereafter, a catheter was inserted in an antecubital vein and the first blood sample was taken, together with collection of a first muscle biopsy of the *m. vastus lateralis.* Exercise was initiated exactly 60 minutes after intake of the capsules. An exercise session started with a 10-minute warm-up at 90% GET, followed by seven intense bouts of three minutes cycling at a power output of 100% RCP + 15% (Δ maximal power – RCP). Intense bouts were interspersed with 3 minutes active recovery at 90% GET and the session ended with 5 min of cooling-down at 90% GET. Water intake was allowed ad libitum during the first session and the same volume was provided for the next 2 sessions. After the exercise bout participants recovered passively by sitting down for 3 h, during which post-exercise measurements were obtained. Muscle biopsies were taken 0 min and 180 min post-exercise and venous blood samples after 0, 30, 60, 120 and 180 min. During the first two hours of recovery, participants ingested 1.2 g/kg BW per hour of carbohydrates in the form of a gel (Nutritional Energy Gel, Etixx Sports Nutrition, Merelbeke, Belgium) and recovery shakes in skimmed milk (Carbo-Gy, Etixx Sports Nutrition, Merelbeke, Belgium), kindly provided by Etixx Sports Nutrition.

H1 and H2 blockade

We employed a single blockade of H1 and H2 receptors with oral, selective antagonists, as similar blockade strategies have been shown to blunt post-exercise hypotension.[80,81] H1 receptors were blocked by administration of 540 mg fexofenadine (Telfast, Sanofi), reaching peak plasma concentrations after ±1 h with a ±12 h elimination half-life.[82] H2 receptors were blocked with 40 mg famotidine (Pepcid, Aurobindo Pharma), with ±2-3 h to peak concentrations and ±3-4 h half-life.[83] All study drugs (fexofenadine, famotidine, and lactose as placebo) were placed in opaque capsules by a lab technician not involved in data collection or analysis. An identical amount of antagonist and placebo capsules that were similar in look further ensured optimal blinding of participants and investigators. For all experiments, participants ingested capsules 1 h before the start of exercise, based on previous research and the pharmacokinetic properties.

Muscle biopsies

After local anaesthesia (0.5 mL of xylocaine, 1% without epinephrine; Aspen Netherlands B.V., Gorinchem, The Netherlands) and a small incision (3-5 mm), a biopsy was taken from the *m. vastus lateralis* using the percutaneous Bergstrom needle biopsy technique with suction.[84] Baseline and immediate post exercise biopsies were taken from the same incision in distal and proximal direction respectively, while for the biopsy during recovery a new incision (more proximal) was made. The leg was randomly chosen on day 1 and was alternated for the 2 other experimental days. One part of the muscle sample was immediately frozen in liquid nitrogen and stored at −80 °C until further analysis. Another part of the muscle sample was stored in RNAlater, held at 4 °C for maximum 3 days for fiber dissections and subsequently frozen at −80°C for RNA isolation.

Histamine release experiments

Microdialysis experiment 1

Interstitial samples were collected before and after 30 minutes of one-legged knee extensor exercise. Histamine concentrations were corrected for probe recovery. Detailed methodology has been described previously.[77,78]

Microdialysis experiment 2

Interstitial samples were collected at rest, during passive exercise, during active exercise and during recovery. More details can be found in Van der Stede et al.,[78] although only samples from the first two active exercise bouts were used. Muscle interstitial fluid was collected from a 20 kDa 63 MD catheter with a 30 mm membrane length (#8010514, MDialysis lab, Stockholm, Sweden). A small amount (1 μL per 10 mL) of glucose D-[3-3H] (#NET331A, PerkinElmer, Waltham, USA) was included in the perfusate, consisting of Ringer-acetate (#468932, Fresenius Kabi, Copenhagen, Denmark), for calculation of probe recovery. The main purpose of this determination of probe recovery was to correct for differences in recovery or perfusion from rest, passive movement to exercise.

Arterial-Venous balance experiment 1

Healthy post-menopausal women performed 30 minutes one-legged knee-extensor exercise with collection of samples from the femoral artery and vein, as described before.[79]

Arterial-Venous balance experiment 2

During the experimental procedures of 'Microdialysis experiment 2', also femoral arterial and venous samples were collected.

Biochemical analysis

UHPLC-MS/MS

All experiments were performed on a Xevo TQ-S MS/MS system with 2.5 μL injection volume, with details described before.[78] The only differences were the used UHPLC solvents for the mobile phase, more specifically solvent A (water + 0.2% formic acid), solvent B (acetonitrile + 0.2% formic acid) and solvent C (200 mM ammonium formate in water) with a starting gradient of 0:95:5 (v:v:v). Histamine (59964), 4-imidazole acetic acid hydrochloride (219991), L-histidine (H8000) and histamine-α,α,β,β-d4 dihydrochloride (762962) were ordered from Merck. N-methylhistamine (19516-10) and 1-methyl-4-imidazole acetic acid hydrochloride (18815-10) were ordered from Sanbio. Sample preparation is also identical to previously published methods,[78] with undiluted samples for microdialysis samples and using histamine-d_4 as internal standard.

Muscle homogenate and lysate preparation

Muscle samples were freeze-dried (48 hours), dissected free from blood, fat, and connective tissue, and divided into two pieces for Western blotting and glycogen synthase activity (4 to 8 mg) and glycogen content (2 to 3 mg). For Western blotting and glycogen synthase activity, freeze-dried muscle samples were homogenized in a fresh batch (1:80 ratio) of ice-cold buffer of pH 7.5 (10% glycerol, 20 mM Na-pyrophosphate, 150 mM NaCl, 50 mM HEPES (pH 7.5), 1% NP-40, 20 mM β-glycerophosphate, 2 mM Na_3VO_4, 10 mM NaF, 2 mM PMSF, 1 mM EDTA (pH 8), 1 mM EGTA (pH 8), 10 μg/mL aprotinin, 10 μg/mL leupeptin, and 3 mM benzamidine) for 1 minute at 30 Hz (Qiagen Tissuelyzer II, Retsch GmbH, Haan, Germany). Then, the homogenates were rotated end over end for 1 h at 4°C and centrifuged for 30 min at 17500 g at 4°C, after which the lysates were aliquoted. Total protein content was determined with a Pierce protein assay kit using BSA standards (#23225, Thermo Scientific, MA, USA).

Muscle glycogen

Muscle glycogen was measured in homogenates after 2 h boiling in 500 μL of 1M hydrochloric acid. Samples were neutralized by 500 μL of 1M sodium hydroxide and glycosyl units were measured by a fluorometric method.[85]

Glycogen synthase activity

Glycogen synthase activity was determined in duplicate in the muscle homogenates with varying concentrations of glucose-6-phosphate (G6P) availability (0.02, 0.17 and 8 mmol/L). The G6P-independent activity (%I form) was calculated as '(activity at

0.02 mmol/L / activity at 8 mmol/L) x 100'. The fractional velocity (%FV) was calculated as '(activity at 0.17 mmol/L / activity at 8 mmol/L) x 100'.

Western blot

Muscle biopsy lysates were diluted to equal protein concentrations in sample buffer (7 mL of 0.5 M Tris-base, 0.93 g dithiothreitol, 1 g sodium dodecyl sulfate, 3 mL glycerol and 1.2 mg bromophenol blue) and double-distilled water. Equal protein amounts were loaded on self-casted SDS-PAGE gels, and with all samples from the same participant on the same gel. A standard sample was loaded in duplicate on every gel to normalize between gels. A standard curve of samples with known protein concentrations were loaded once for each protein to verify linearity of band intensity. Proteins were separated by gel electrophoresis and semi-dry transferred to PVDF membranes (Immobilon Transfer Membrane, Millipore, MA, USA). Membranes were blocked for 30 minutes at room temperature and incubated with primary antibodies over-night at 4 °C. The following day, membranes were washed for 3x5 min in tris-buffered saline with 0.1% Tween 20 (TBST) and incubated with horseradish peroxidase-conjugated secondary antibodies (Jackson ImmunoResearch, Ely, UK) for 1 h at room temperature. After washing three times in TBST for 5 min, the membrane was visualized with chemiluminescence (Millipore, MA, USA) on a ChemiDoc MP imaging system (Bio-Rad Laboratories, CA, USA). After visualization, membranes were stained for total protein content to verify equal loading and transfer (#24585, Pierce Reversible Protein Stain Kit, Thermo Scientific, MA, USA). No membranes were stripped or re-probed. Band quantification was performed with Image Lab (Bio-Rad Laboratories, CA, USA) and protein content was calculated in arbitrary units normalized to the band intensity of the average of the standard samples on every gel. Phosphorylated levels were then normalized to the total content of the respective protein (except for STAT3), and normalized to the baseline values.

Plasma glucose and insulin levels

Blood was collected in sodium fluoride coated tubes (BD Vacutainer, Becton Dickinson, New Jersey, USA), followed by immediate centrifugation (5 min at 3000 g) and storage at -80 °C until analysis. Glucose (Architect c, Abbott) and insulin (Cobas e801, Roche Diagnostics) levels were determined in the lab for clinical biology at Ghent University Hospital.

Circulating immune cells

Venous blood (K3 EDTA, Vacutest Kima) from an antecubital vein was collected at pre-exercise and each of the recovery time points, stored at 4 °C and analyzed within 6-8 hours. Blood samples were analyzed for concentrations of leukocytes, including lymphocytes, monocytes, neutrophils, basophils and eosinophils using an automated hematology analyzer (SYSMEX XN-1000, Sysmex Corporations) at the WADA-accredited Doping Control Laboratory in Ghent.

RNAscope

Cryosections (10 μm) of young, healthy individuals (n = 3) were used for RNAscope fluorescent detection of histamine receptors, histidine decarboxylase and cell type markers. The RNAscope multiplex fluorescent reagent kit v2 (#323285, Advanced Cell Diagnostics, Inc) was used according to the manufacturer's instructions, with probes against *HRH1* (#416501-C3), *HRH2* (#416511-C2), *HDC* (#311441), *TPSB2* (#577161-C2), *FOLR2* (#1286201-C1), *CD1C* (#514761), *SLC11A1* (#543541), *PDGFRA* (#604481), *PECAM1* (#487381) and *ACTA2* (#444771). Targets were fluorescently labelled with TSA Vivid fluorophore 520 (1:1000, PN 323271), 570 (1:1000, PN 323272) or 650 (1:1500, PN 323273). Immediately after the last washing step, sections were incubated for 20 min at room temperature with wheat germ agglutinin to identify the muscle fiber membranes (1:25, CF®770 WGA, Biotium, #290059), followed by 30 s counterstaining with DAPI (D1306, Invitrogen). Slides were then covered with Prolong Gold Antifade Mountant (P10144, Invitrogen), dried overnight at room temperature and subsequently stored in the dark at 4 °C. The slides were then imaged using a fluorescence microscope with a ×20 objective (Zeiss Axioscan 7, Zeiss) and images were processed in QuPath (v. 0.5.1).

Single-fiber RNA sequencing

The detailed workflow of our single-fiber transcriptomics methodology has been described before.[19]

Fiber isolations

Muscle biopsy chunks were submerged in RNAlater in a petri dish and individual muscle fibers (25 from each biopsy, 3150 fibers in total) were manually dissected under a light microscope using fine forceps. Immediately after dissection, fibers were incubated in 3 μL of SingleShot Cell Lysis kit (Bio-Rad) at room temperature (10 min), 37 °C (5 min) and 75 °C (5 min) (T100, Bio-Rad), with removal of DNA (DNase enzyme) and proteins (proteinase K). Lysates were then stored at -80 °C until further processing.

Sequencing

Illumina-compatible polyA+ libraries were generated from 2 μL of muscle fiber lysates using the QuantSeq-Pool 3' mRNA-Seq library prep kit (Lexogen). Unique Molecular Identifiers (UMIs) and sample-specific i1 indices were added during the first step of reverse transcription, to allow for sample pooling in the downstream process. After sample pooling, RNA removal, second strand synthesis (random priming) and i5/i7 index addition, libraries were purified, amplified and purified again. Quality of the libraries was assessed with a high sensitivity small DNA Fragment Analysis kit (Agilent Technologies, DNF-477-0500). Libraries were then sequenced on a NovaSeq 6000 instrument with a NovaSeq S2 kit (100 cycles), with loading of 2 nM pools. Sequencing quality control metrics included a 61-76% of clusters passing filter, 96% clusters occupied and an 89.2% Q30, with 4099 million total reads.

Initial data processing

Read data underwent quality control and was demultiplexed, trimmed, aligned, deduplicated and counted, according to the Lexogen QuantSeq Pool pipeline (https://github.com/Lexogen-Tools/quantseqpool_analysis). The count matrix was then transformed into a Seurat object for further processing.[86]

Bulk muscle RNA sequencing

RNA isolation and gDNA removal

Total RNA from the muscle biopsies (approx. 25 mg wet weight) stored in RNAlater was extracted using a miRNeasy Mini kit (#217004, Qiagen) according to the manufacturer's instructions. RNA concentrations were quantified using a NanoDrop instrument after which all samples were diluted to equal RNA concentrations. Removal of gDNA was then performed with a HL-dsDNase kit (#70800, ArcticZymes) with 20 ng total RNA as input in an 8 μL reaction.

Library preparation and sequencing

DNase-treated RNA (8 μL) was then used for total RNA sequencing library preparation using a SMARTer Stranded Total RNA-Seq Kit (v3 - Pico Input Mammalian, #634487, Takara) with AMPure XP Beads. Manufacturer's instructions were followed, with fragmentation (4 min at 94 °C) included in the cDNA synthesis step and five and twelve cycles during the PCR1 and PCR2 steps, respectively. SMARTer RNA Unique Dual Index Kit – 96U Set A (#634452, Takara) and Set B (#634457, Takara) were used to allow sequencing of all samples in one pool. Quality of all libraries was verified using a KAPA qPCR kit (concentration of libraries, in quadruplicate) and Fragment Analyzer (library size distributions). Libraries were then equimolarly (100 nM per sample) pooled into one final pool used for sequencing. The libraries were then sequenced using a NovaSeq S2 kit (2 x 100 nucleotides) on a NovaSeq 6000 instrument with loading of 0.65 nM (1% Phix).

Primary data processing

Adapter trimming was performed using cutadapt (*v. 1.16*) and UMI counts were extracted with UMItools (*v. 1.0.0*). Reads were then mapped to the human genome using STAR (*v. 2.7.3a*) and invalid UMIs were removed with an in-house developed Python script. Error rate on spikes were determined with fgbio (*v. 1.0.0*) and UMIs were added as UM tags in the BAM files. HTSeq (*v. 1.15*) was then used for counting of the alignments. Quality control was performed at several intermediate steps with FastQC (*v. 0.11.*9).

Single-cell RNA sequencing

Detailed methodology of the used dataset has been described previously.[22] Gastrocnemius muscle samples were collected from peripheral artery disease (PAD) patients (n = 4) and non-PAD participants (n = 4). Metabolically active (Calcein^{+}) mononuclear cells were FACS sorted and underwent single-cell RNA sequencing using the Chromium Next GEM Single Cell 3' Reagent kit (v3.1, 10x Genomics). For all analyses in this paper, only cells from the non-PAD participants were used (n = 37333 cells). Low quality cells were discarded based on library size (total sum of UMI counts detected per cell), number of detected genes and percentage of reads mapped to mitochondrial genes. Doublets were identified and removed in every sample using runDoubletFinder from the singleCellTK (v. 2.6.0) package.

Combined H1/H2 blockade RNA sequencing

RNA sequencing data and associated metadata was downloaded from the Gene Expression Omnibus website (GSE71972).

Bioinformatics

Single-fiber quality control

Filtering and quality control were performed for each condition (placebo, H1, H2) separately. Fibers with less than 1000 UMI counts or 1000 detected genes were deleted. All fibers from one participant were deleted for each condition (different participant for each condition), since very few fibers remained for this participant at one of the timepoints. Next, low abundant genes were filtered with as threshold double the number of fibers in the smallest group (fiber type and timepoint combination). For fiber typing, genes with specific slow (*MYH7*, *TPM3*, *TNNT1*, *ATP2A2*, *TNNC1*, *TNNI1*) and fast (*MYH2*, *TPM1*, *TNNT3*, *ATP2A1*, *TNNC2*, *TNNI2*) isoforms were extracted, followed by calculation of proportions of each slow-fast combination. These proportions were ranked from high to low for each isoform and the bottom knee of that curve was mathematically calculated using the *barcodeRanks()* function from the *DropletUtils* package (v. 1.20.0). Fibers were then classified as slow if all 6 genes classified a fiber as slow and maximal 2 genes as fast, or vice versa. Other fibers were annotated as hybrid fibers. After all quality control and filtering, 912 (placebo), 929 (H1) and 969 (H2) fibers were retained in each dataset. Count normalization was then performed with the *SCTransform()* v2 method in Seurat.[87]

Single-fiber differential expression analysis

For the single-fiber datasets, differential expression analysis was performed using a pseudobulk approach, important to avoid inflated p-values.[88] Pseudobulk aggregation was performed using the *to_pseudobulk()* function from the *Libra* package (v. 1.0.0). *DESeq2* (v. 1.40.2) was then used for the analysis with a 'subject + time' (fiber type independent) statistical model. Technical variation in the form of surrogate variables was modelled with the *num.sv(method = 'be')* and *svaseq()* functions from the *sva* (v. 3.48.0) package. Zero surrogate variables were identified. For significance testing, we used a posteriori fusion scheme integrating fold changes (biological relevance) and p-values (statistical relevance) with a cut-off of 0.05,[89] as used before in -omics skeletal muscle research.[9,90]

Bulk differential expression analysis

The participant that was deleted in the single-fiber analysis for the placebo condition was also deleted in the bulk muscle dataset. One additional sample from pre-exercise was omitted from the analysis based on quality control (principal component analysis and hierarchical clustering). Other steps in the differential expression analysis were identical to the single-fiber analysis. No surrogate variables were identified with the *sva* analysis for the placebo-only comparisons. For the combined analysis with H1 and H2 blockade, the statistical model also included a factor representing library preparation batch and two surrogate variables. The same significance testing strategy was applied to ensure a fair comparison, which also resulted in fewer DEGs compared to using the standard adjusted p-value cut-off.

Feature overlap

Common features or DE features were visualized using the *eulerr* (v. 7.0.0) or *circlize* (v. 0.4.15) packages. For the bulk versus single-fiber comparison, log-transformed raw counts were correlated with the cor.test() function with 'spearman' method. To compare the biotype of detected features, the biotype for each gene was accessed using the *select()* function from the *AnnotationDbi* (v. 1.62.2) with the *EnsDb.Hsapiens.v86* dataset.

Gene set enrichment analysis

The human Hallmark gene sets were accessed via the *msigdbr* (v. 7.5.1) package. Differential expression results were ranked by the Wald statistic and the analysis was performed with the *GSEA()* function in *clusterProfiler* with Benjamini-Hochberg p-value adjustment and the 'fgsea' method.

Biological pathway activity inference

The top 500 interactions per pathway were retrieved from the weighted pathway information in the PROGENy model with the *get_progeny()* function from the *decoupleR* (v. 2.6.0) package. DE lists containing all genes ranked by the Wald statistic were as input in the *run_mlm()* function for the actual inference analysis. Heatmaps were created with the *pheatmap* (v. 1.0.12) package.

Transcription factor activity inference

Differential expression results for the comparisons of input were loaded and used as input, ordered by the 'stat' value from DESeq2. All human regulons were retrieved from the *CollecTRI* and transcription factor activity was inferred via the *run_ulm()* function from the decoupleR (v. 2.6.0) package.

Principal component analysis

Single-fiber PCA was performed on the SCTransformed and scaled data with the *prcomp(center = FALSE, scale. = FALSE)* function. The fiber type independent pseudobulked single-fiber data was transformed into a DESeq2 object followed by variance stabilization using the *vst()* function. The PCA plot was then produced with the *plotPCA()* function on the vst data. The identical approach was applied to the bulk dataset, with the addition of pre-filtering of low abundant genes (only genes with at least 13 samples with a count of 10 or higher).

Single-fiber and -cell integration

The previously published single-cell dataset[22] was integrated with our single-fiber dataset from biopsies at rest.[19] From the single-cell dataset and after quality control, PAD samples were filtered out and all cells per control participant were extracted separately, excluding the myonuclei which are the result of incomplete digestion of multinucleated muscle cells. Cells were normalized separately for each sample with the *NormalizeData()* function from Seurat. This same initial processing step was performed on the single-fiber data, but with fibers from all participants together. These individual Seurat objects were combined and variable features were selected with the *SelectIntegrationFeatures()* function. The objects were then merged with the *merge()* function and the previously determined variable features were assigned to this merged Seurat object. Data was then scaled with *ScaleData()* while regressing out percent of counts associated with mitochondrial genes, followed by PCA analysis with *RunPCA()*. The Seurat object was then integrated using *Harmony* (v. 0.1.1), followed by UMAP calculation and clustering using the first 20 principal components. Individual clusters were then annotated based on well-known marker genes for different cell types. Subclustering of the macrophages/monocytes cluster was performed by applying the exact same pipeline after extracting only the cell ID's associated with these clusters. Significance testing for expression of genes in specific cell types was performed using the *FindMarkers()* function with a minimal log fold-change threshold of 0.25.

CellChat

The workflow of CellChat (v. 2.0.0) was followed,[91] as described in the CellChat repository (https://github.com/jinworks/CellChat). Projection of gene expression onto the protein-protein interaction (PPI) network was not used.

NicheNet

Macrophages, dendritic cells, monocytes, neutrophils and mast cells were selected as sender cells, whilst muscle fibers independent of fiber type were considered as receiver cells. The NicheNet (v. 2.0.4) workflow[36] as described in their repository (https://github.com/saeyslab/nichenetr) was then applied to our dataset. Gene sets of interest were based on the differential expression results from our pseudobulked myofiber analysis per timepoint (i.e., post-exercise and recovery). A stringent cut-off of 33% was used to identify expressed genes in receiver and sender cells. The top 30 active ligands per timepoint were used for receptor network inference.

QUANTIFICATION AND STATISTICAL ANALYSIS

Individual datapoints and mean values are presented in the figures (SEM for Figure 5B), with sample sizes specified in the relevant figure captions. Non-bioinformatic statistical analysis was performed using a linear mixed model approach with the *lme4* package (v. 1.1-34) in RStudio. The model was created using the *lmer()* function for each outcome variable with participant as random effect and fixed effects depending on the experiment (e.g. 'exercise'). Homoscedasticity was checked for the model residuals, and the outcome variable was log-normalized if needed. To check significance of main or interaction effects, the full model was compared with a reduced model, not containing the factor of interest, by the *anova()* function. Pairwise comparisons were performed using the *emmeans()* function from the *emmeans* package (v. 1.8.8) with tukey adjustment for multiple comparisons.